Enhancing Mechanical Strength of Electrospun Nanofibers by Thermal Crosslinking and Coaxial Electrospinning

by

Scott A. O. Smith

A thesis

presented to the University of Waterloo

in fulfillment of the

thesis requirement for the degree of

Master of Applied Science

in

Mechanical and Mechatronics Engineering

Waterloo, Ontario, Canada, 2023

Author’s Declaration

I hereby declare that I am the sole author of this thesis. This is a true copy of the thesis, including any required final revisions, as accepted by my examiners.

I understand that my thesis may be made electronically available to the public.

Abstract

Electrospinning of nonwoven nanofibrous mats has received significant attention in recent years due to the high versatility and porosity of electrospun mats. Specifically, considerable interest has developed in using electrospun nanofiber mats as breathable dressing layers, separator layers in lithium-ion batteries, etc. For example, the high porosity and high pore interconnectivity of nanofiber mats allows them to exhibit superior electrochemical characteristics and high overall battery performance. However, electrospun mats generally suffer from poor mechanical strength, creating the risk of a short circuit if a rip or tear were to appear.

Many methods exist to improve the mechanical strength of electrospun nanofiber mats. Composite structures, such as multilayer or coaxial mats, can be used to improve the average mechanical strength of the fibers, while post-treatments can be used to improve the inter-fiber bonding to increase mechanical strength. However, many of these techniques impact the complexity and scalability of electrospinning or impact physical properties such as porosity. Alternatively, thermal crosslinking of fibers by heat treatment has emerged as a simple, scalable method of significantly improving mechanical strength, but typically results in considerable shrinkage.

In this work, coaxial electrospinning is combined with thermal treatment to produce a novel method of improving the mechanical strength of nanofiber mats, without incurring significant dimensional shrinkage. Coaxial PAN/PVDF-HFP mats showed no significant shrinkage when tested at temperatures up to 240 ºC for 20 minutes, compared to the homogenous PVDF-HFP mats, which displayed a shrinkage of 94% when treated at 190 ºC for 20 minutes. When treated at 178 ºC for up to 30 minutes, the coaxial fibers consistently showed changes in thickness of less than 10% and no significant change in area. More importantly, the reductions in thickness and volume experienced by the coaxial mats were much more uniform across the varied treatment times when compared to those of the homogenous PVDF-HFP samples. The as-spun coaxial fibers showed a decrease in porosity compared to homogenous PVDF-HFP (95% to 79%) but remained much more porous than the commercial PP separator (41%). In addition, no significant change in average porosity in the coaxial samples occurred following treatment at 178 ºC for 20 minutes. Coaxial samples heat treated at 178 ºC for 5 minutes demonstrated a mechanical strength of 7.72 MPa, a 22% increase when compared to the as-spun coaxial fibers, and a 54% increase compared to the as-spun homogenous PVDF-HFP. Elongation at break decreased from 17.8% to 5.3% following the 5-minute heat treatment, showing a significant reduction compared to the elongation at break for as-spun PVDF-HFP (79.7%), and PVDF-HFP treated at 178 ºC for 5 minutes (40.6%). Therefore, the proposed technique of combining heat treatment with coaxial morphologies demonstrates significant potential for improving mechanical strength without dimensional shrinkage.

Acknowledgements

As I submit this thesis, I would like to take the opportunity to thank all the people who have supported and guided me through its writing.

I would first like to thank my supervisor, Professor Zhongchao Tan, for all the time, oversight, and guidance he has invested in me for the last two years. His experience and wisdom have allowed me to learn what it means to be a scientific researcher and I appreciate his dedication in helping me to reach my goal.

I must also thank Professor Norman Zhou and Mr. Jansen Zhou for allowing me access to their testing equipment. Without them, these results would not be possible.

Next, I would like to express my appreciation to my fellow researchers, Dr. Yifu Li and Mr. Yi Zhang, and all the other past and present members of the Green Energy & Pollution Control Research Lab at the University of Waterloo. The mentorship and assistance I received from these individuals was invaluable to me in the completion of this thesis. I will always remember the time and effort they invested in me.

Finally, I must thank my friends and family, who supported me throughout this time in my life. Without their guidance, love, and companionship I would not be the person I am today, and I will always be eternally grateful to them for their part in my achievement. Specifically, I thank my closest friends; Emily, Christopher, and Sandon, for standing by me during these last two years and making them some of the best times in my life.

Table of Contents

List of Figures

List of Tables

Nomenclature

Notation	Term
6FBAPP	2,2-bis[4-(4-aminophenoxy)phenyl]hexafuoropropane
BPA	Bisphenol A
BPDA	3,3’,4,4’-biphenyl tetracarboxylic dianhydride
DCM	Dichloromethane
DMAc	Dimethylacetamide
DMF	Dimethylformamide
DNA	deoxyribonucleic acid
ODA	4,4’-oxydianiline
OPS	Octaphenyl-polyhedral oligomeric silsesquioxane
PAA	polyacrylic acid
PAN	Polyacrylonitrile
PBS	polybutylene succinate
PCL	Polycaprolactone
PDA	Polydiacetylene
PE	Polyethylene
PEO	Polyethylene oxide
PI	Polyimide
PLA	Polylactic acid
PLGA	Polylactic-co-glycolic acid
PMIA	Poly(m-phenylene isopthalamide)
PP	Polypropylene
PPESK	Poly(phthalazinone ether sulfone ketone)
PVDF	Polyvinylidene fluoride
PVDF-HFP	Polyvinylidene fluoride-co-hexafluoropropylene
PVP	Polyvinylpyrrolidone
SiO_2	Silicone dioxide
TiO_2	Titanium dioxide

Chapter 1
Introduction

1.1 Background

In 1964, Geoffrey Taylor first characterized the stable conical deformation that occurs in a droplet of liquid when a sufficient electric charge is applied to it. [1] During this process, the charge buildup within the droplet causes electrostatic repulsion forces to act against the surface tension of the droplet. This results in the destabilization of the droplet shape as it elongates and quickly trends towards a conical shape known as a Taylor cone. As the strength of the electric field continues to increase, a jet of liquid forms at the tip, which later becomes a fiber. [2]

In the 1990s, Darrell Reneker produced a variety of micron and nanoscale organic polymer fibers using an electrospinning technique which has become ubiquitous in the subsequent decades. [3, 4] This technique consisted of filling a glass capillary tube with a polymer solution and inserting a metal electrode. Hydrostatic pressure was applied to the capillary tube to produce a stable droplet at the tip of the tube, and a high voltage was applied to the metal electrode to produce a charge in the solution droplet. The elongated polymer jet ejected from the droplet was then collected by various grounded screens to form fiber mats once the solvent had been evaporated. [3] Using this technique, Reneker was able to produce polyethylene oxide (PEO) fibers ranging from 50 nm to 5 μm in diameter; he also identified a number of critical experimental parameters of the electrospinning process including viscosity, conductivity, surface tension, electric potential, collector distance, temperature, humidity, and air velocity. [3] Continuing from this work, Reneker was able to electrospin micro- and nanofibers using polyimides (PI), polyamic acid (PAA), nylon, polyacrylonitrile (PAN), and deoxyribonucleic acid (DNA), demonstrating the versatility of the technique. [5]

A typical modern electrospinning system has made several improvements to Reneker's original method as seen in Figure 1.1. The glass capillary and metal electrode are typically replaced with a syringe with a small-diameter metallic needle or spinneret, and a syringe pump has replaced Reneker's system of air valves to maintain the correct hydrostatic pressure. The addition of a rotating collector, such as a rotating drum or conveyor, allows one to control the degree of orientation of the deposited fibers by adjusting rotation speed, and allows for a more uniform deposition over a larger collection area. [6] Multi-needle and needle-less electrospinning processes can be used to significantly increase the nanofiber deposition rate compared to single needle electrospinning, [7] and multi-needle [8] or coaxial [9] electrospinning can be used to create composite electrospun nanofiber mats.

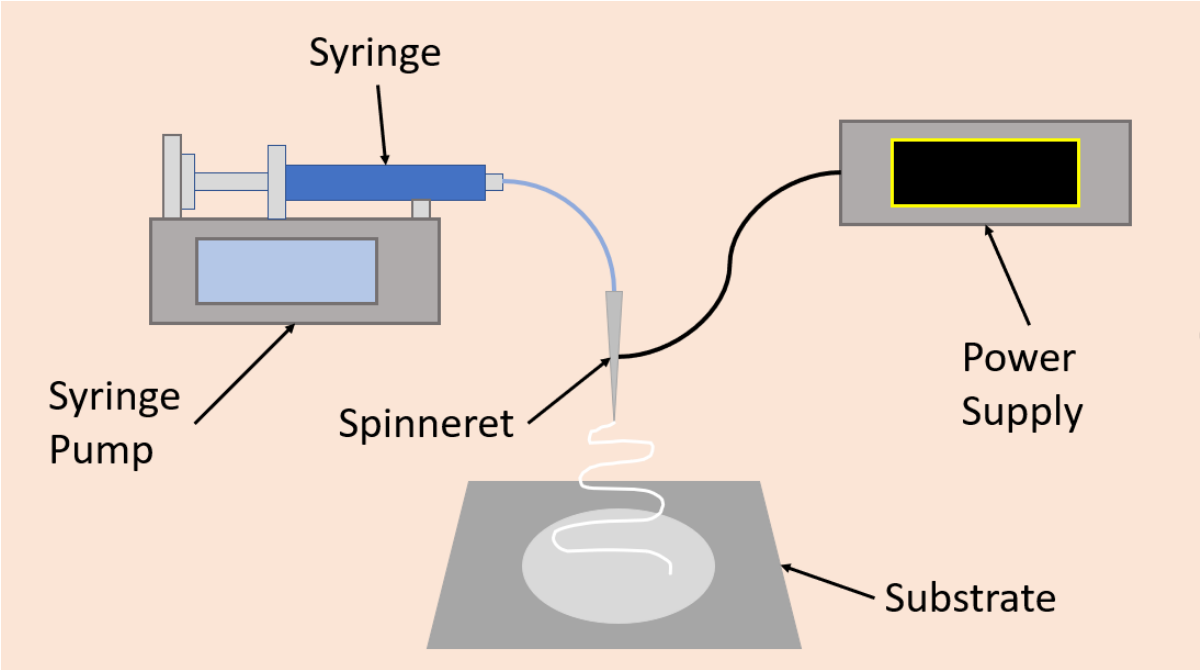

Figure 1.1 Typical Electrospinning Configuration

1.2 Motivations and Challenges

Recently, much research has been performed in our group to produce electrospun nanofibers for different applications, including air filtration, lithium-ion battery separator, and surface dressing. [10-25] The high surface area, high porosity, great pore connectivity, and versatile material choice of electrospun nanofibers allows them be used effectively as scaffolding or materials for lithium-ion battery electrodes. [26] Electrospun nanofibers are especially attractive for use as battery separator layers because of their large specific surface areas, pore interconnectivity, and surface wettability [27, 28].

Traditional battery separators used in industry are commonly observed to have many undesirable qualities. As opposed to the pores of electrospun nanofibrous mats which consist of the interstitial spaces between fibers, the pore structure in commercial microporous separators are produced by stretching hot and cold mats, which results in pore shape and mechanical strength being strongly aligned with the machine direction. [29] As a result, commercial separators possess low porosities, typically between 40-60%, which result in higher internal resistances, lower permeability, and lower overall battery performance. [30] Commercial separators also exhibit poor thermal stability, displaying significant shrinkage at temperatures of 90 ºC. [30, 31] Electrospun nanofibers, therefore, are an attractive alternative.

However, adoption of electrospun nanofiber separators has been hindered by their generally poor mechanical strength. Single polymer electrospun separator layers have been recorded to have lower mechanical performance than that of commercial separators. [32] As a result, separator layers must be made thicker to accommodate low mechanical strengths for safe operation. However, thicker separators result in higher internal resistances, and lower energy densities. [33] Separator layers that fail under mechanical loading, or shrink under thermal loading, cannot separate battery electrodes, leading to short-circuits and possible fires. [34]

Techniques exist to improve the mechanical strength of electrospun nanofiber nonwoven mats, but these often result in drawbacks to their functionality. Several of these techniques are discussed in depth in Chapter 2, however thermal crosslinking via heat treatment emerges as a highly effective, yet extremely simple and straight-forward technique for improving the mechanical strength of an electrospun nanofiber mat. However, this increase is often accompanied by a significant dimensional shrinkage although heat treatment can produce significant increases in mechanical strength. [35]

Evidently, there is a need to develop a method of heat treating of nanofiber mats without experiencing significant shrinkage. As discussed in Chapter 2, coaxial electrospinning can be used to produce composite nanofibers with great thermal stability for use in lithium-ion batteries. It therefore follows that this technique could similarly be used to improve the thermal stability of the nanofiber mats during heat treatment to allow for thermal crosslinking of the outer layer without widespread structural shrinkage. Therefore, the purpose of this thesis is to investigate and characterize the difference in behaviour of homogenous and coaxial nanofiber mats under heat treatment.

1.3 Research Objectives

This study aims to investigate the implementation of a coaxial morphology to mitigate the dimensional shrinkage typically experienced by electrospun nanofiber nonwoven mats under heat treatment. This will be accomplished by producing both homogenous and coaxial PAN/polyvinylidene fluoride (PVDF) nanofibers and subjecting them to identical rounds of testing to identify differences in behaviour due to heat treatment.

The goals of this thesis work are therefore:

1) Develop a technology to improve the mechanical strength of nonwoven nanofiber mats without loss of structure
2) Evaluate the performance of the technology developed

To achieve these goals, the following steps are taken:

1) Fabrication and characterization of thermally crosslinked PAN/PVDF core/sheath nanofibers
2) Evaluation of the performance of thermally crosslinked PAN/PVDF core/sheath nanofibers

1.4 Thesis Structure

The thesis is structured as follows: Chapter 1 introduces the history and basics of electrospinning as a method of producing function nanomaterials; it also introduces the motivation for the study. Chapter 2 serves as a literature review on the current methods of producing and improving functional electrospun nanofiber mats with a focus on mechanical strength. Chapter 3 describes the methodology of the experiments carried out in this thesis work. Details are provided regarding solution and experiment parameters used during production of nanofibers, and the equipment and procedures used during testing. Chapter 4 details the experimental results of this thesis work. Chapter 5 presents conclusions and recommendations for future research based on the results and data presented in Chapter 4.

Chapter 2
Literature Review

2.1 Monolayer Separators

The monolayer separator represents the simplest construction available for electrospun nanofiber mats. It is produced using a single polymer precursor without any additional modification to structure during or post deposition, and results in a randomly distributed nanofiber mat characterized by high porosity, electrolyte uptake, and ionic conductivity. [32] Polyvinylidene fluoride (PVDF), PAN, and polyimide (PI) are the most commonly used polymers for the production of monolayer separators [12] due to their high mechanical strength, desirable surface characteristics, and electrochemical stability. [33]

Choi *et al.* [36] demonstrated that the physical and mechanical characteristics of electrospun PVDF fiber mats were highly dependent on the solvent parameters of the polymer solution used. The study observed that larger proportions of dimethylacetamide (DMAc) in a mixed Acetone/DMAc solvent mixture resulted in high solution viscosity, small average pore size, and small average fiber diameter. Higher weight concentrations of DMAc in the solvent mixture corresponded to an increase in Young's modulus in the samples, with an increase from 8.46 MPa to 29.7 MPa as DMAc concentration was increased from 0% to 50%. The maximum strength of the samples increased from 3.37 MPa to 7.58 MPa and the maximum strain increased from 117% 273% as DMAc concentration was increased from 0% to 20%. The authors theorized that a decrease in fiber diameters resulted in greater inter-fiber bonding due to a larger number of crosslinking points, with the solidity of the fiber-fiber bonding being dependent on the evaporation behaviour during electrospinning.

Widiyanadari *et al*. [37] investigated the effects of the applied voltage during the electrospinning process on the nanofiber morphology and mat structure. The data indicated that higher applied voltages resulted in less uniform nanofibers, and the formation of fibers with beaded morphologies. The study also demonstrated that higher voltages were responsible for producing nanofiber mats with lower porosities, as the porosities of the mats fell from 93% to 86% as voltage was increased from 13 kV to 17 kV.

Castkova *et al.* [38] also demonstrated the effects of applied voltage on fiber diameter and morphology. The results indicated that a higher applied voltage resulted in both a significantly smaller average fiber diameter as well as a significantly smaller fiber diameter distribution. The mean fiber diameter decreased from 1343 nm to 678 nm, as applied voltage was increased from 25 kV to 50 kV at a distance of 20 cm while also resulting in a substantially reduced range of diameters at the higher voltage.

Zaarour *et al.* [39] investigated the influence of PVDF molecular weight on mechanical properties for aligned nanofiber mats. This study suggested that mechanical properties universally increase with an increase in molecular weight. When the molecular weight of the samples was increased from 180,000 to 530,000 the ultimate tensile strength of the samples increased from 7.9 MPa to 10.78 MPa, the strain at break increased from 35 to 48%, and Young's modulus increased from 32.6 MPa to 82.73 MPa. This was accompanied by a significant increase in the measured diameters of the fibers that was attributed to an increase in solution viscosity that resulted in increased evaporation times for the solvent solutions.

Miao *et al.* [40] demonstrated the significantly superior thermal and electrochemical characteristics of a nonwoven PI electrospun mat compared to the commercial Celgard battery separator. The PI nonwoven separator displayed an onset temperature of degradation of over 500 ºC, significantly above the melting point of the polypropylene (PP) Celgard mat at 167 ºC. When heat treated at 150 ºC for 1 hour, the PI mats demonstrated no shrinkage or discoloration while the Celgard mat experienced significant shrinkage. The PI mats also demonstrated a superior capacity retention ratio when discharged at high current densities. The PI retained 90% of its capacity retention at 1C, 70% at 5C, and 62% at 10C; while the Celgard mat retained 80%, 56%, and 45% respectively at the same current densities.

Cheng *et al.* [41] measured the tensile strength of aligned 3,3',4,4'-biphenyl tetracarboxylic dianhydride-2,2-bis[4-(4-aminophenoxy)phenyl]hexafuoropropane polyimide (BPDA-6FBAPP PI) nanofiber sheets at 308 MPa, and Chen *et al.* [42] measured the tensile strength of aligned BPDA-bisphenol A (BPDA-BPA) and BPDA-4,4'-oxydianiline (BPDA-ODA) PI nanofiber sheets at 384 MPa and 459 MPa, respectively. This allows the electrospun mats to exceed the recorded mechanical strength of the commercial Celgard polypropylene separator (175.4 MPa in the machine direction and 12.6 MPa in the transverse direction), as measured elsewhere in literature. [43] However, PI polymers are immiscible and cannot be electrospun directly. PI nanofibers must be prepared by electrospinning polyacrylic acid (PAA) nanofiber precursor which must then be imidized at a high temperature. [12]

2.2 Modified Separators

The mechanical, electrochemical, and thermal properties of electrospun nanofiber mats can be further augmented by implementing post-deposition modifications to their structures. Several thermal and chemical processes can be performed to improve the fiber-fiber bonding in the electrospun mats to improve mechanical performance.

Dip-coating, the method of immersing a separator into a coating solution to allow the material to adhere to the surface, is the most widely applied method to modify electrospun nanofiber separator layers. [12] Shi *et al.* [44] investigated a method for dip-coating electrospun polyvinylidene fluoride-co-hexafluoropropylene (PVDF-HFP) electrospun separator mats in polydiacetylene (PDA) solution. The

dip-coating of the samples caused bonding at overlapping fiber junctions resulting in an increase in mechanical strength from 7.1 MPa to 11.2 MPa in the dry state. Dip-coating also resulted in a decrease in porosity from 77.7% to 72.8% and an increase in electrolyte uptake from 206% to 254%. The dip-coated samples also displayed significantly improved thermal stability, with only gradual shrinkage up to 200ºC, compared to a commercial PP separator which melted at 160ºC and the pure PVDF-HFP sample which melted at 170ºC.

The mechanical performance of nonwoven mats can be greatly improved via hot-pressing, where the mat is subjected to both elevated temperatures and compressive forces to melt and flatten the nanofibers to encourage welding at the fiber joints. However, this method is also typically accompanied by a significant impact on mat porosity. [12] Jiang *et al.* [45] performed a hot-pressing of PI nanofiber mats to improve their mechanical strength. The mechanical strength of the mats was increased from 12 MPa to 31 MPa as the pressure of the pressing treatment was increased from 1 MPa to 5 MPa. The electrospun mats experienced no shrinkage due to the hot pressing, however, porosity was significantly reduced from 87% to 73% and electrolyte uptake from 340% to 270% as the pressing pressure was increased from 1 MPa to 5 MPa.

Alternatively, samples can be heat treated in a circulating oven or uniform bath to achieve thermal crosslinking of fibers with less significant impact on porosity at the cost of a greater degree of area shrinkage in the samples. Lee *et al.* [46] demonstrated a technique for heat treating electrospun nanofiber mats in Pluronic F127 to reduce the effect of shrinkage. Polycaprolactone (PCL) scaffolds which were placed in a pre-warmed bath at 55ºC for 30 minutes had their mechanical strengths increased from 5.1 MPa to 9.1 MPa and their elongation at break increased from 417% to 675%, without any significant change to fiber diameter or pore area. Additionally, samples which were heat treated in Pluronic F127 maintained over 80% of their original dimensions, compared to approximately 25% for samples treated in water. Rozent *et al.* [47] demonstrated that the primary cause of deformation during heating of ceramic doped polyvinylpyrrolidone (PVP) nanofibers was nonuniform relaxation of the stretched polymer fibers. The study indicated that shrinkage caused by thermal treatment began at approximately 100ºC, far below the polymer decomposition temperature, and accelerated at temperatures above the polymer's glass transition point. The study found that this behaviour could be prevented by slow pre-firing and sintering at 750ºC, resulting in calcination of the nanofiber mat without significant change to size or structure.

Crosslinking of fibers to improve the mechanical strength of the nonwoven mats can also be accomplished by chemical rather than thermal means. Li *et al.* [48] demonstrated a method for chemically crosslinking PCL and polylactic-co-glycolic acid (PLGA) nanofiber mats via exposure to the solvent dichloromethane (DCM) at varying partial pressures and exposure times. This method resulted in an increase in tensile strength and Young's modules of the PCL mats from 11.5 MPa to 21.4

MPa and 8.41 MPa to 16.5 MPa, respectively, without any significant change in structure, porosity, or fiber diameter. The PLGA mats exhibited an increase in tensile strength from 9.93 MPa to 15.01 MPa without any major change to fiber or mat structure.

2.3 Composite Separators

2.3.1 Multilayer separators

Multilayer separators can be manufactured by successive rounds of electrospinning onto a single substrate. By combining multiple layers of different polymers or materials it is possible to create a separator that shares the benefits of each. It is common to use a reinforcing polymer in a two- or three-layer multilayer separator to augment the mechanical or thermal properties of a nanofiber mat which already possesses good surface characteristics. [12]

By introducing a reinforcing layer of high-strength poly(m-phenylene isopthalamide) (PMIA) electrospun nanofibers between two layers of PVDF, Zhai *et al*. [49] were able to significantly increase the mechanical strength of their sample from 9.97 MPa for homogenous PVDF to 13.96 MPa for their tri-layer structure. Similarly, Liu *et al.* [50] demonstrated significant increases in mechanical strength in a tri-layer separator consisting of a traditional polyethylene (PE) mat reinforced by two exterior layers of PI. This PI/PE/PI separator showed an increased mechanical strength of 177.6 MPa, compared to a typical mechanical strength of 150 MPa for traditional PE based mats while maintaining a similar elongation at break of 40.16%.

Multilayer separators can also be designed to have a polymer layer serve as a shutdown layer. One of the constituent layers would possess a lower melting point, so that the layer would fully melt and block the pores of the separator in the event of a short-circuit to halt the chemical reaction. [12] Wu *et al.* [51] successfully designed a PI/PVDF/PI trilayer separator for this purpose. This multilayer separator demonstrated the described melting behaviour at 170º C, which resulted in a reduction to 7% of normal cell operating capacity, indicating a severe blockage of the separator pores due to the PVDF layer melting. However, the separator exhibits a shrinkage of only 2.2% and 2.7% at thermal treatments of 90ºC and 160ºC, compared to 2.7% and 5.4% for the commercial PP separator, due to the reinforcement of the exterior PI layers. The thermal shutdown point of the cell also resides above that of the commercial PE separator, which begins to melt at 130ºC. When heat treated for 2 hours at 180ºC, the PI/PVDF/PI separator showed 2.7% shrinkage while the commercial PP separator showed severe melting and distortion.

2.3.2 Copolymers

Copolymers are produced by the direct blending of two or more polymers to achieve a final product with the shared characteristics of its constituent parts. Copolymers have become ubiquitous in the field of electrospinning due to their improved mechanical, chemical, and thermal characteristics when compared to their base polymer. The copolymers of PVDF, especially PVDF-HFP (which demonstrates improved flexibility compared to PVDF) [32], have been widely used and studied due to their high mechanical strength and good stability. [52]

Kundu *et al.* [53] demonstrated that the PVDF-HFP copolymer possessed a higher β-phase content and electrolyte uptake than the base PVDF polymer. When tested in a half-cell the copolymer also demonstrated both higher capacity and greater capacity retention. Zhu *et al.* [54] blended PVDF and PAN to form a functional copolymer which, when electrospun, demonstrated superior mechanical and thermal capabilities to the pure PVDF nanofiber mats. After undergoing heat treatment, the blended nanofibers of equal-parts PVDF/PAN possessed an ultimate tensile strength of 20.4 MPa, substantially higher than either the pure PVDF or PAN nanofiber mats which both possessed mechanical strengths of less than 10 MPa. The blended copolymer also demonstrated thermal stability and electrolyte uptake greater than that of the pure PVDF nanofibers but less than that of the pure PAN fibers.

2.3.3 Co-electrospinning

Co-electrospinning, or co-spinning, is the process by which multiple polymers with complimentary properties are simultaneously electrospun from multiple separate needles onto a shared substrate or collector. This allows the polymer nanofibers to mix freely in the nonwoven mat, which combines the advantages of each while allowing the nanofibers to maintain their own raw properties. [12]

Chen *et al.* [8] produced a composite PVDF-HFP/PI bicomponent mat via co-electrospinning that then underwent thermal calendaring at 135ºC for 3 minutes. This heating process caused the PVDF-HFP fibers in the cross-spun mat to melt and fuse to the PI fibers at the joints to improve the mechanical strength of the mat. This technique increased the mechanical strength of the combined mat from 2 MPa to 7.5 MPa after thermal calendaring. The thermal stability of this mat was shown to be superior to that of the commercial Celgard membrane. Both were heat treated at 180ºC for 30 minutes, the bicomponent electrospun mat showed no significant deformation while the Celgard mat shrunk by 40%.

Cai *et al.* [55] expanded on this technique by producing both a conventional co-spun PVDF-HFP/PI bicomponent mat and a second bicomponent PVDF-HFP/PI mat by side-by-side electrospinning. This process is similar to cross-electrospinning except the respective needles are placed close enough together that the Taylor cones are allowed to mix and interact such that the resulting polymer jet is comprised of both polymer streams. The results of this study indicate that the side-by-side bicomponent

mat possessed superior mechanical capabilities, demonstrating a mechanical strength of 7.08 MPa compared to the 5.91 MPa tensile strength of the conventional cross-electrospun mat.

2.3.4 Coaxial Electrospinning

Coaxial, or core-sheath, composite nanofibers can be created by electrospinning with two coaxially aligned needles. The core material of the coaxial fiber typically provides mechanical or thermal stability to the fiber structure, while the sheath material provides desirable surface characteristics such as electrolyte affinity. [12]

Huang *et al.* [56] developed a coaxial nanofiber morphology with an exterior PVDF-HFP sheath and an inner cellulose core recycled from a cigarette filter. This coaxial fiber mat demonstrated a tensile strength of 34.1 MPa, compared to an experimentally measured value of 35.9 MPa for the commercial Celgard 2300 mat. The measured tensile strength of the mats increased from 27 to 34.1 MPa as the cellulose content in the mats was increased from 61-79%. After a 1-hour treatment at 200ºC, the composite and pure cellulose mats showed no significant shrinkage, while the pure PVDF-HFP mat showed minor shrinkage, and the commercial Celgard mat showed a shrinkage of 85%. The composite PVDF-HFP/cellulose mat also demonstrated the best flame retarding ability, especially compared to the Celgard and pure cellulose mats, which caught fire within 2 seconds of exposure to an open flame.

Jiang *et al.* [57] developed a coaxial polylactic acid (PLA)/ polybutylene succinate (PBS) nanofiber mat to serve as thermal shutdown layer, similar to multilayer separators. After treatment at 130ºC for 30 seconds, the PLA/PBS separator showed total occlusion of the pores, corresponding to complete melting of the PBS sheath and shutdown of the chemical reaction. The thermally and mechanically stable PLA core showed no change in dimensions during this heat treatment, allowing it to maintain the dimensional profile of the separator layer and prevent leakage.

Gong *et al.* [58] produced a high strength coaxial mat by hot-pressing electrospun poly(phthalazinone ether sulfone ketone) (PPESK)/PVDF core/sheath nanofibers. The mechanical strength of the mat was significantly increased after being hot pressed at 170ºC and 2MPa for 1 hour, from 3.5 MPa to 23.2 MPa. However, due to the exterior PVDF shell melting, the porosity of the sample was reduced from 88% to 65% and the electrolyte uptake was reduced from 960% to 585%. The coaxial PPESK/PVDF samples also demonstrated no significant shrinkage at treatment temperatures up to 200ºC while the commercial PP separator showed obvious shrinkage at 150ºC and at 170ºC began becoming transparent due to melting.

2.3.5 Nanoparticles

The mechanical and electrochemical profiles of electrospun nanofiber separators can also be further enhanced by incorporating nanoparticles into their precursor solutions. Yanilmaz *et al.* [59] incorporated titanium dioxide (TiO_2) and silicone dioxide (SiO_2) nanoparticles into electrospun nylon 6,6 nanofiber mats. The inclusion of the nanoparticles resulted in a decrease in average fiber diameter from 463 nm to 312 nm for TiO_2 doped nanofibers, and 218 nm for SiO_2 doped nanofibers. The mechanical strength of the nanofibers was increased from 18 MPa to approximately 22 MPa for both types of nanoparticles. Chen *et al.* [60] produced composite PVDF electrospun nanofibers containing organic-inorganic Octaphenyl-polyhedral oligomeric silsesquioxane (OPS) nanoparticles, which showed significantly improved thermal and mechanical properties. The inclusion of organic-inorganic nanoparticles resulted in an increase in mechanical strength from 1.6 MPa for the pure PVDF mat to 12.7MPa with the inclusion of 2% OPS. When heat treated at 150ºC for 2 hours the samples showed a reduction from 4.3% to 0.5% shrinkage with the inclusion of 1% OPS and no observable shrinkage in any samples with larger inclusions of OPS.

2.4 Summary

The electrospinning technique provides a method of creating highly porous samples with desirable surface characteristics which are well suited to operate as separator mats in lithium-ion batteries.

Monolayer separators represent the simplest method of producing electrospun mats and possess high porosities, interconnected pore structures, and large specific surface areas. The wide selection of electro-spinnable polymers allows for a variety of electrospun monolayer separators with good mechanical and surface properties. However, the generally low mechanical strength of unmodified monolayer separators lowers their desirability due to the risk of shrinkage or deformation which could cause dangerous short circuits in the batteries.

Monolayer separators can be modified to significantly improve their mechanical performance and their feasibility as separator layers. Dip-coating allows for significant augmentations to the electrochemical surface characteristics of the separator layers while also providing a moderate increase in mechanical strength. Hot-pressing allows for a significant increase in the mechanical strength of electrospun mats at the risk of significant reductions in porosity and changes to mat structure. Chemical crosslinking allows for potentially significant increases in mechanical without significant changes to structure but requires a solvent solution to be tailored to the nanofiber mat. Conventional heat treatment represents the simplest and most scalable method of modification, and allows for significant increases in mechanical strength, without significant impact on porosity or fiber diameter, but carries a significant risk of sample shrinkage.

Composite separators similarly allow for significant augmentations to the performance of electrospun separators. Multilayers, copolymers, coaxial fibers, and cross spinning all allow for the incorporation of two or more complimentary polymer components to significantly reinforce the thermal or mechanical behaviour of the nanofiber mat. The insertion of nanoparticles into the polymer solutions similarly allows for significant improvements to mechanical and electrochemical properties.

Importantly, the introduction of a composite morphology into an electrospun nanofiber separator could be used to improve the mechanical and thermal profile of the sample to compensate for the trade-offs typically experienced by the above modifications. A coaxial structure could be selected to provide a thermally stable reinforcing frame to a polymer with desirable surface characteristics. This would allow the fibers to overcome the thermal deformation that is characteristic of heat treatment techniques and improve the viability of an otherwise simple and scalable technique for improving mechanical strength. A coaxial morphology would allow for full surface coverage of the outer sheath, minimizing the impact of a bi-component structure on the electrochemical properties of the surface and the ability of the outer layer to bind to other fibers during heat treatment. A coaxial morphology will therefore be adopted in this work to mitigate the effects of thermal heat treatment to investigate this highly scalable method of producing sufficiently mechanically strong fibers for use as battery separators.

Chapter 3
Methodology

3.1 Materials

Polyacrylonitrile (PAN, Mw 150000), Polyvinylidene fluoride-hexafluoropropylene (PVDF-HFP, Mw 455000), Dimethylformamide (DMF, 99.8% purity), and n-butyl-alcohol (N-butanol, 99.5% purity) were purchased from Sigma Aldrich (Canada). Acetone (99.8% purity) was purchased from Fisher Scientific (USA). All chemicals were used as purchased without modification.

3.2 Preparation and Fabrication of Samples

3.2.1 Homogenous PVDF Nanofibers

PVDF-HFP polymer was dissolved in a solvent mixture comprised of acetone and DMF in a 7:3 ratio by mass to create a precursor solution of 12% mass concentration. This solution was extruded through a 21-gauge syringe at a distance of 11cm onto a rotational drum collector rotating at 20rpm and coated in a non-stick aluminium foil substrate. A voltage of 9kV was applied to the solution at a constant flowrate of 1.25mL/hr. All nanofiber production was carried out between 21 to 23 degrees Celsius and 20% to 45% relative humidity.

3.2.2 Coaxial PAN/PVDF Nanofibers

PVDF-HFP polymer was dissolved in a solvent mixture comprised of acetone and DMF in a 3:7 ratio by mass to create a sheath precursor solution of 12% mass concentration. PAN polymer was dissolved in pure DMF to create a 10% mass concentration solution. The PAN solution was extruded within the interior 22-gauge syringe at a rate of 0.6mL/hr, while the PVDF-HFP solution was extruded between the interior 22-gauge syringe and an exterior 15-gauge syringe at a rate of 0.9mL/hr. A voltage of 7.5kV was applied to the syringe at 11cm from a drum collector rotating at 20rpm. All nanofiber production was carried out between 21 to 23 degrees Celsius and 20% to 45% relative humidity.

3.2.3 Heat Treatment

Samples were divided into approximately 2cm by 2cm squares in batches of five. These samples were then heat treated in batches of 5 in an isothermal oven (Precision Compact Oven, Thermo Fisher Scientific, USA). Tensile test samples were treated at 178ºC for between 5 to 30 minutes. Porosity samples were treated at 178ºC for 20 minutes. Additional samples were treated individually from 160ºC up to 240ºC to assess the thermal stability of the electrospun mats. 178ºC was selected as the primary treatment temperature using the results determined in Appendix A. Mechanical strength was identified

to increase with increases in treatment temperatures, however fiber destabilized at temperatures above 180ºC. 178ºC was therefore selected as the maximum acceptable temperature due to fluctuations in oven temperature.

3.3 Sample Characterization

3.3.1 Morphology

The morphology of the samples was analyzed using an ESEM (Quanta Feg 250 ESEM, FEI, USA) to collect high-resolution photos of the samples. These images were then imported into a computational software (MATLAB, Mathworks, USA) to calculate the fiber diameter distribution using a method described previously in literature. [61]

3.3.2 Shrinkage Measurement

The thicknesses of the electrospun mats were measured in five locations before and after heat treatment using a digital caliper to measure the effect of the heat treatment. The areas of the mats were measured digitally before and after heat treatment by analyzing images of the samples using an image processing software (ImageJ, Eliceiri, USA). Total volume change was calculated using measurements for both area and thickness.

3.3.3 Porosity and Electrolyte Uptake

The porosity and electrolyte uptake of the samples were evaluated using a butanol-uptake test. As-spun and heat treated samples were weighed before being soaked in n-butyl-alcohol for 2 hours. The samples were then dried on a measuring paper and weighed again.

The porosity is calculated using Eq. 3.1 (3.1):

$$\alpha = (W_w - W_d)/(\rho_b \cdot V) \tag{3.1}$$

where α, W_d and W_w represent the porosity, dry weight and wet weight of the samples, ρ_b represents the density of n-butanol, and V is the geometric volume of the sample.

The electrolyte uptake (ϵ) is calculated using Eq. 3.2:

$$\epsilon = \frac{W_w - W_d}{W_d} \cdot 100\% \quad (3.2)$$

3.3.4 Tensile Strength

The tensile strength of the samples was evaluated using a UTM device (5548 Micro-Tester, Instron, USA). The samples were tested until failure. The stress and strain were calculated using the data from the UTM and the measured dimensions of the samples. An alternative means of calculating mat thickness was used for samples where the thickness of the mat varied by more than 100% between the thinnest and thickest regions. In this case, the three thinnest adjacent measurements were used to calculate the average mat thickness as this was consistently observed to correlate strongly to the regions of failure in the samples.

Chapter 4
Results and Discussion

4.1 Morphology

Figure 4.1 shows the SEM images of the electrospun PVDF-HFP and coaxial PAN/PVDF-HFP nanofiber mats. The coaxial mat shows a clear core/sheath morphology, with a continuous and separate inner core of PAN within the outer PVDF-HFP layer. The coaxial fibers demonstrate a more heavily beaded morphology than the PVDF-HFP fibers which are largely smooth and uniform. The fiber diameter distributions of the as-spun homogenous PVDF-HFP and coaxial PAN/PVDF-HFP mats are shown below in Figure 4.2. The homogenous and coaxial mats possess an average fiber diameter of 1236 nm and 1499 nm, respectively. The bimodal distribution of the coaxial fiber diameters, with peaks at 500 nm and 1300 nm, is representative of the difference in diameters between the fibers and beads. Both types of fiber demonstrate heavy-tailed distributions with significant percentages of fibers above 2500 nm.

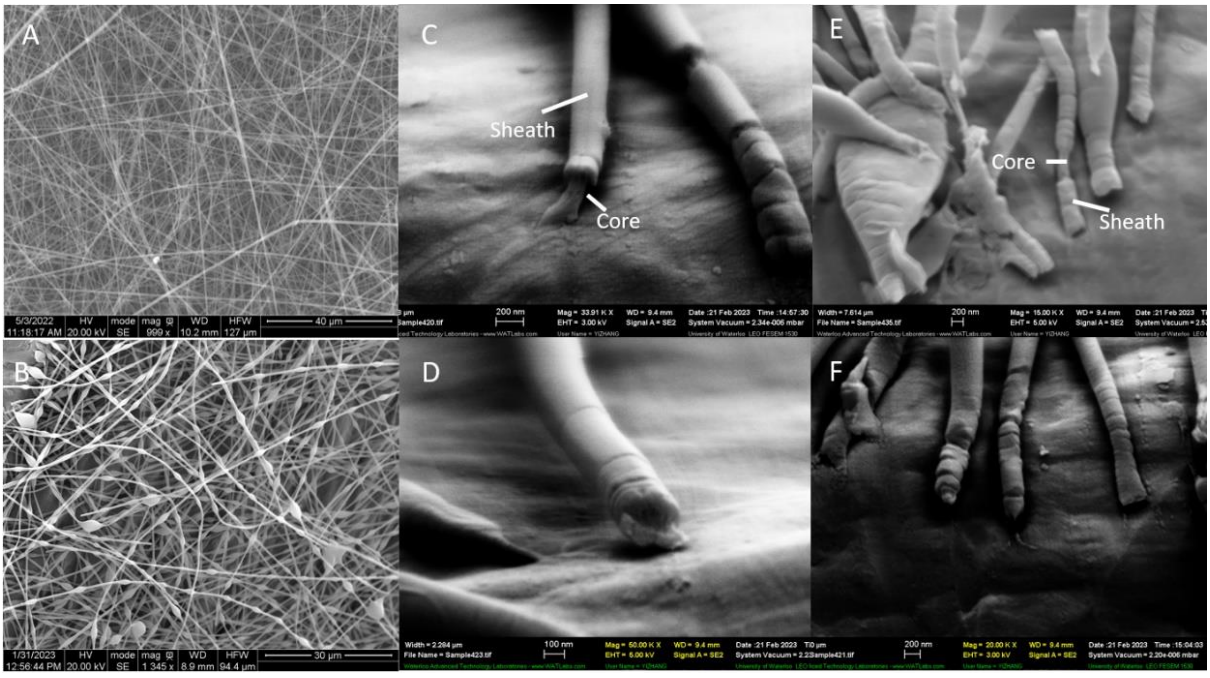

Figure 4.1 SEM Images of A) Homogenous PVDF-HFP Mat B) Coaxial PAN/PVDF-HFP Mat C-F) Coaxial Core/Sheath Structure

The beaded morphology of the coaxial PAN/PVDF-HFP fibers indicates that the chain entanglement of the polymer solution was insufficient to overcome the Rayleigh instability of the electric field. [62] McKee *et al.* [63] demonstrated that the chain entanglement of a polymer solution was dependent on the weight concentrations of the polymers, designating the minimum concentration required to produce beaded fibers as C_e. The study also showed that the critical concentration required to prevent the formation of beads was approximately equal to twice that of C_e. Shenoy *et al.* [64] further investigated this relationship, identifying that the entanglement number of a solution was dependent on both polymer weight concentration and molecular weight. A minimum entanglement value of 2 was required to produce beaded fibers, and a minimum value of 3.5 was required to produce smooth fibers. Increased weight concentration also resulted in larger fiber diameters. Zhang *et al.* [65] demonstrated a similar behaviour for homogenous nanofibers, where an increase in PVA weight concentration from 6% to 8% resulted in an increase in average nanofiber diameter from 87 nm to 246 nm. Greater applied voltages were also demonstrated to result in larger fiber diameter distributions.

Recent research has shown that the morphology of the inner polymer core of the coaxial nanofibers is dependent on the flowrate ratio between the core and sheath polymers. Wang *et al.* [66] demonstrated that the greater the outer flowrate, the greater the outer diameter of the fiber, and the greater the inner flowrate, the greater the diameter of the inner core and the thinner the outer polymer layer. Too low of an inner flowrate will prevent the formation of a continuous core, and too high an inner flowrate will result in the inner polymer escaping the Taylor cone as a separate polymer jet.

Therefore, a smoother morphology could be achieved in the coaxial nanofibers by increasing both the molecular weight and the weight concentrations of PAN and PVDF-HFP within the solution, in order to overcome the Rayleigh instability. Additionally, the outer diameter of the coaxial fibers and wall thickness of the outer layer could be more closely controlled by adjusting the total and relative flowrates of the core and sheath polymers. This could be used to identify an optimal combination for achieving maximum mechanical strength, while maintaining a sufficient structural core to prevent shrinkage during heat treatment. It can also be seen that the larger average diameters of the coaxial mats are most likely a result of their higher total solution flowrate (1.5 mL/hr compared to 1.25 mL/hr) and the larger fiber diameter distribution of the homogenous fibers are likely a result of their higher applied voltage (9 kV compared to 7.5 kV). These parameters could be controlled to produce thinner fibers to improve mechanical performance, as fiber diameter have been shown to affect both individual fiber strength [38] and inter-fiber bonding [36].

These results clearly show that the PAN/PVDF-HFP samples demonstrate an obvious coaxial structure with a sufficient outer sheath to allow for thermal crosslinking. Additionally, the beaded morphology of the coaxial fibers results in greater surface roughness [67] and lower porosity [37] which result in greater mechanical strength in the nanofiber mat, as is shown in section 4.4.

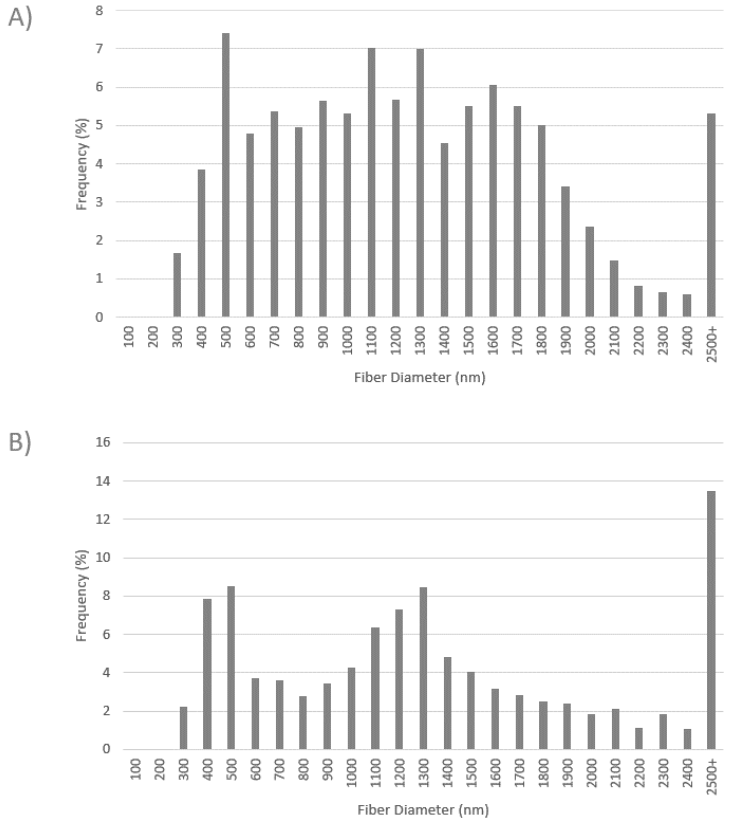

Figure 4.2: Fiber diameter distribution of as-spun A) homogenous PVDF-HFP and B) coaxial PAN/PVDF-HFP mats

4.2 Thermal Stability and Shrinkage Characterization

Figure 4.3 shows the images of the homogenous PVDF-HFP and coaxial PAN/PVDF-HFP nanofiber mats before and after heat treatment at increasing temperatures. The PVDF-HFP sample experiences rapid shrinking as the temperature is raised above 180 ºC, displaying a reduction in area of approximately 94%. Conversely, the coaxial PAN/PVDF-HFP sample shows no significant signs of shrinkage at temperatures as high as 240 ºC, although a slight discoloration is visible in the sample treated at 230 ºC, and more noticeably in the sample treated at 240 ºC.

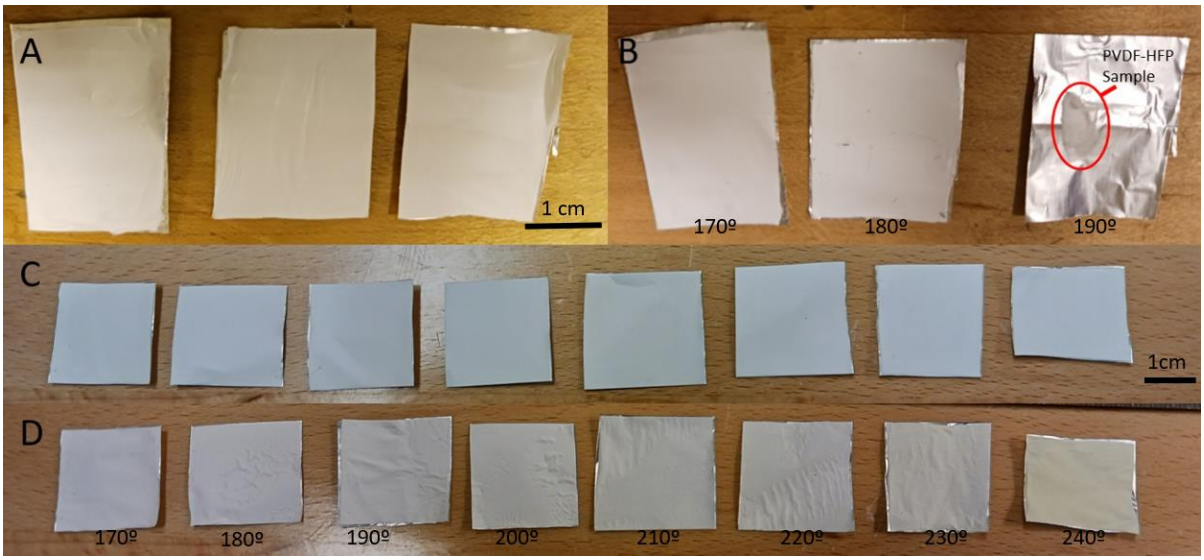

Figure 4.3 Images of samples before and after heat treatment for 20 minutes at increments of 10 ºC A) PVDF-HFP before treatment at 170º-190º B) PVDF-HFP after treatment at 170º-190º C) PAN/PVDF-HFP before treatment at 170º-240º D) PAN/PVDF-HFP after treatment at 170º-240º

The level of shrinkage observed in the heat treated mats is very similar to what has been reported elsewhere in literature. Shi *et al*. [44] reported that a PVDF-HFP mat experienced a loss of most of its area, accompanied by a color change from white to transparent, due to obvious melting after being heat treated at 170 ºC for 30 minutes. Zhu *et al.* [54] similarly reported complete shrinkage of a pure PVDF-HFP mat after being treated at 200 ºC for 30 minutes, in contrast to a pure PAN mat which experienced no reduction in area and partial discoloration. Wei *et al.* [68] demonstrated that minor shrinkage below the polymer bonding temperature was the result of molecular chain relaxation in amorphous regions of the fibers, while the abrupt and significant shrinkage that occurs at higher temperatures coincided with the melting of small crystal structures within the polymer.

The discoloration of the coaxial samples after undergoing heat treatment is indicative of the oxidative stabilization that PAN undergoes between 200 ºC and 300 ºC. [69] PAN was demonstrated by Gupta *et al.* [70] to melt at temperatures above 300 ºC, with higher melting points observed for greater heater rates. The study observed that the melting point of PAN increased from 340º to 365 ºC as the heating rate was increased from 80 ºC to 160 ºC per minute, primarily due to temperature lag. As such, the lack of significant shrinkage in the coaxial PAN/PVDF-HFP mats can therefore be attributed to the PAN nanofiber core retaining its physical structure due to its significantly higher thermal stability.

Figure 4.4 shows the proportional change in thickness of the homogenous PVDF-HFP and coaxial PAN/PVDF-HFP samples after undergoing heat treatment at 178 ºC for between 5 and 30 minutes. The homogenous PVDF-HFP samples demonstrate a range of behavior as treatment time is increased, displaying both positive and negative changes in mat thickness, while the coaxial PAN/PVDF-HFP mats demonstrate a consistent, linear change in thickness. Additionally, the changes in proportional thickness observed in the homogenous mats are significantly greater than those observed in the coaxial fibers. The pure PVDF-HFP samples experience proportional changes up to approximately 15% of their original thickness, while the PAN/PVDF-HFP mats experience a reduction in thickness of less than 8% at all measured treatment durations. Neither the coaxial nor homogenous samples experienced any loss of mass during heat treatment.

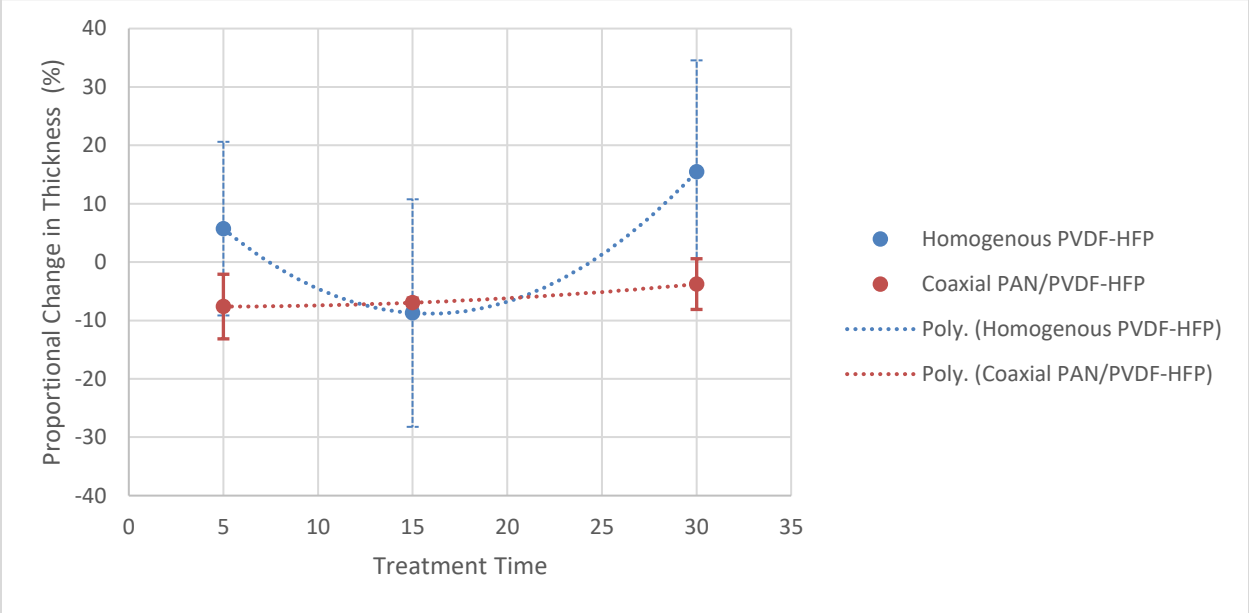

Figure 4.4 Proportional change in mat thickness in homogenous PVDF-HFP and coaxial PAN/PVDF-HFP samples treated at 178 ºC for between 5 and 30 minutes

The proportional change in total mat volume due to heat treatment can be seen in Figure 4.5. As the coaxial PAN/PVDF-HFP mats experienced no reduction in area, the total volume change displayed in Figure 4.5 is equivalent to the change in mat thickness displayed in Figure 4.4. The homogenous PVDF-HFP samples experienced a moderate decrease in mat thickness after being treated at 178 ºC for up to 15 minutes, then experienced a significant increase in thickness as treatment times were increased to 30 minutes. Conversely, the coaxial PAN/PVDF-HFP mats demonstrate a small reduction in volume due to heat treatment which trends towards zero as treatment times increase.

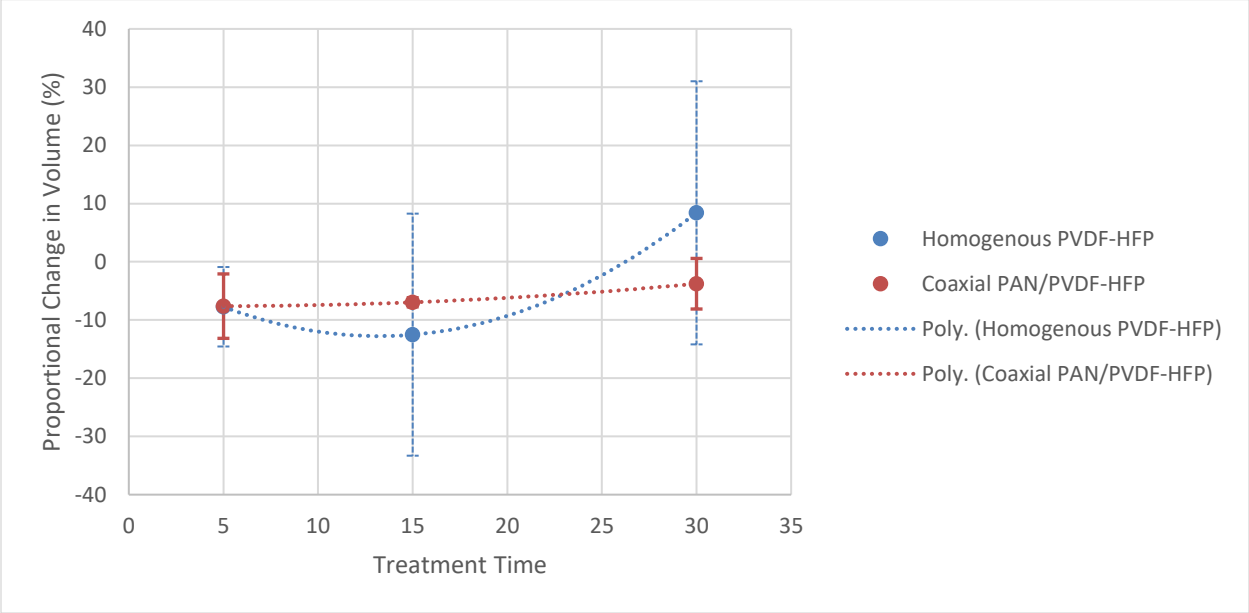

Figure 4.5 Proportional change in total mat volume in homogenous PVDF-HFP and coaxial PAN/PVDF-HFP samples treated at 178 ºC for between 5 and 30 minutes

Wei *et al.* [68] demonstrated a similar trend in fiber mat thickness caused by heat treatment, where thickness first moderately decreased then significantly increased, as treatment temperatures increased. The study indicated that the initial reduction in thickness was caused by chain relaxation in amorphous regions of the fiber. However, this was counteracted by more significant melting behaviour at higher temperatures, which resulted in linear shrinkage of the fibers and increases in average fiber diameter - which coincides closely with the behaviour observed in the homogenous PVDF-HFP mats. This trend in mat thickness indicates the high rate of heating, due to the use of a preheated oven, results in a temperature lag, which is only resolved at higher treatment times. Elishav *et al.* [71] similarly found that heat treatment of electrospun polymers resulted in the thermal relaxation of internal stresses. These stresses are the result of stretching, caused by the whipping of the polymer jet during the electrospinning process. This linear shrinkage along the nanofiber results in a decrease in length and an increase in fiber diameter, resulting in a decrease in mat area and an increase in average mat thickness. This explains why the change in thickness of the electrospun PVDF-HFP mats is greater than the corresponding change in volume, as the increase in thickness is partially offset by the reduction in area.

However, this behaviour is not reflected in the change in volume observed by the coaxial PAN/PVDF-HFP fibers. Instead, the change in thickness of the coaxial fibers strongly resembles the results reported by Cipriani *et al.* [69] where homogenous PAN nanofibers experienced a reduction in fiber diameter of

less than 15% after being treated at 250 ºC for 30 minutes. The coaxial mats do not experience the significant increase in thickness caused by linear shrinkage from melting, and more closely resemble the shrinkage behaviour of pure PAN. It can therefore be concluded that the inter-fiber structure of the coaxial nanofiber mat is successfully maintained by the PAN core, which possesses a melting point significantly above the treated temperature. The gradual increase in mat thickness observed in the coaxial fibers can potentially be attributed to linear shrinkage in the exterior PVDF-HFP sheath, resulting in minor increases in average fiber diameter and mat thickness.

4.3 Porosity

The change in porosity and electrolyte uptake experienced by the homogenous and coaxial samples after undergoing heat treatment is shown in Table 1. The as-spun coaxial PAN/PVDF-HFP mats demonstrate a significantly lower porosity compared to the as-spun PVDF-HFP mats (79.4% and 95.6%, respectively), while maintaining a comparable electrolyte uptake (217% and 224%, respectively). Widiyandari *et al.* [37] recorded a similar loss of porosity from 93% to 86% due to the introduction of beads to PVDF nanofiber mats, resulting from an increase in applied voltage during electrospinning. Thus, the beaded morphology of the coaxial mats could be considered a significant factor in the differences in porosity between homogenous and coaxial mats.

After being heat treated at 178 ºC for 20 minutes, the coaxial sample demonstrates a minor increase in porosity (79.4% to 83.4%), while the homogenous PVDF-HFP sample demonstrates a minor decrease in porosity (95.6% to 91.6%). Both fiber morphologies demonstrate porosities far exceeding that of the Celgard 2400 monolayer PP battery separator, which possesses a porosity of only 41%, as reported by the manufacturer. Both the homogenous and coaxial samples demonstrate major increases in electrolyte uptake after undergoing heat treatment (294.1% and 260.3%, respectively) - significantly outperforming the Celgard 2400 separator, which was reported to have an electrolyte uptake of only 81%. [27] This increase in electrolyte uptake is not fully understood at this time, as it is not accompanied by a comparable increase in porosity. However, it can clearly be seen that the coaxial PAN/PVDF-HFP structure prevents any significant decrease in porosity due to heat treatment. Indicating that the PAN core is successful in maintaining the structure of the nanofiber mat.

Table 1 Porosity and Electrolyte Uptake of homogenous PVDF-HFP and coaxial PAN/PVDF-HFP samples treated at 178 ºC for 20 minutes

Sample	**Porosity (%)**	**Electrolyte Uptake (%)**
PVDF-HFP As-Spun	95.6 $\pm$ 10.4	224 $\pm$ 14.8
PVDF-HFP 20 Minute Treatment	91.6 $\pm$ 13.9	294.1 $\pm$ 55.2
Coaxial PAN/PVDF-HFP As-Spun	79.4 $\pm$ 11.8	217 $\pm$ 29.9
Coaxial PAN/PVDF-HFP 20 Minute Treatment	83.4 $\pm$ 23.1	260.3 $\pm$ 46.4

4.4 Tensile Strength

The mechanical properties of the homogenous PVDF-HFP and coaxial PAN/PVDF-HFP nanofiber mats, before and after heat treatment, are shown in Table 2. The mechanical strength of the coaxial PAN/PVDF-HFP nanofiber mat (6.33 MPa) is 26% greater than that of the homogenous PVDF-HFP nanofiber mat (5.05 MPa), as-spun. After being treated at 178 ºC for 5 minutes, the mechanical strength of the coaxial nanofiber mats was increased by approximately 22% (to 7.72 MPa) relative to the as-spun coaxial sample, resulting in a 54% margin compared to the as-spun homogenous sample. However, the mechanical strength of the coaxial mats after their heat treatment remains less than that of the homogenous PVDF-HFP sample after receiving a 5-minute treatment (10.38 MPa).

The coaxial PAN/PVDF-HFP samples also demonstrate considerably lower elongation at break compared to the homogenous PVDF-HFP nanofiber mats. The coaxial samples demonstrate approximately 22% of the elongation at break of the homogenous samples as-spun and approximately 13% after being heat treated at 178 ºC for 5 minutes. The elongation at break of the coaxial samples is more strongly affected by the heat treatment process, showing a 70.2% (17.8% to 5.3%) decrease after the 5-minute heat treatment compared to a 49.1% decrease (79.8% to 40.6%) for the homogenous PVDF-HFP samples.

Table 2 Mechanical properties of homogenous and coaxial fibers before and after heat treatment at 178C

Material	Treatment	Tensile Strength (MPa)	Elongation at break (%)
PVDF-HFP	As-Spun	5.02 ± 1.54	79.76 ± 26.60
	5 Minute (178ºC)	10.38 ± 3.55	40.60 ± 25.61
	15 Minute (178ºC)	10.20 ± 2.88	37.78 ± 4.54
	30 Minute (178ºC)	9.60 ± 2.17	30.22 ± 2.24
Coaxial	As-Spun	6.33 ± 0.53	17.79 ± 12.43
	5 Minute (178ºC)	7.72 ± 1.19	5.30 ± 2.81
	15 Minute (178ºC)	7.90 ± 1.70	5.04 ± 1.83
	30 Minute (178ºC)	7.43 ± 1.12	6.17 ± 2.69

The mechanical strength of the mats decreases at longer treatment times, with homogenous and coaxial samples decreasing by 3.8% (7.43 MPa) and 7.5% (9.60 MPa) respectively, as treatment times increase from 5 minutes to 30 minutes. The homogenous PVDF-HFP samples demonstrate a corresponding 25% reduction in elongation at break as treatment time is increased from 5 minutes to 30 minutes, however the coaxial PAN/PVDF-HFP samples instead demonstrate a 16% increase in elongation at break as treatment time is increased from 5 minutes to 30 minutes.

As shown in Figure 4.6, the as-spun homogenous PVDF-HFP sample demonstrates a very small region of elastic deformation, with the plastic region representing most of the deformation in the sample. Conversely, the heat treated samples demonstrate more significant elastic regions and much steeper slopes in the plastic region. Tensile strength and failure mechanics differ greatly between the heat treated and as-spun samples. The sample which underwent heat treatment for 5 minutes experiences a sudden rupture, while the as-spun sample instead experiences an extended necking behaviour which accounts for more than 60% of the total strain. As the duration of heat treatment increases, the slope of the plastic region increases, resulting in increasingly higher ultimate tensile strengths and lower elongations at break among the samples.

The changes in mat strengths and failure mechanisms are likely due to changes in the loading of fibers within the electrospun mats. Chavoshnejad *et al.* [72] demonstrated that, in nanofiber mats which have not been thermally crosslinked, the load is experienced only by the fibers which span the full distance over which the load is being applied, while the remaining fibers have little to no contribution. As the degree of fiber bonding increases due to thermal treatment, the loading of the nanofiber mat is split more evenly amongst the fibers in the mat, resulting in higher mechanical strength. This leads to a change in failure mechanism, as the higher stress results in a cascade of fiber failures as the applied load exceeds the mechanical strength of the individual fibers. As such, higher degrees of bonding result in higher mechanical strengths and lower elongation at break.

Therefore, the significant necking behaviour in the as-spun mats, shown in Figure 4.6, can be considered a result of the applied force overcoming the weak inter-fiber bonding, causing the remaining fibers to be pulled apart after the initial load-bearing fibers fail. After receiving heat treatment, the nanofiber mats demonstrate the typical increase in mechanical strength and decrease in elongation that is characteristic of thermal crosslinking. As such, the degree of inter-fiber bonding clearly increases with increased treatment times.

The mechanical behaviour of the coaxial PAN/PVDF-HFP mats under load are shown in Figure 4.7. The coaxial mats demonstrate significantly more developed elastic regions of deformation and significantly lower elongations at break compared to the homogenous PVDF-HFP samples. Interestingly, the coaxial PAN/PVDF-HFP mats also demonstrate a lower mechanical strength post

heat treatment as shown in Table 2 and Figure 4.6, despite possessing a higher mechanical strength as-spun. The as-spun coaxial sample demonstrates a significantly steeper slope in the elastic region compared to the as-spun homogenous mat, and demonstrates a relatively small region of necking behaviour followed by a sudden break. This indicates a much higher degree of inter-fiber bonding is present in the as-spun coaxial mat than in the as-spun homogenous mat, most likely due to increased surface roughness caused by the beaded morphology of the coaxial fibers. [67]

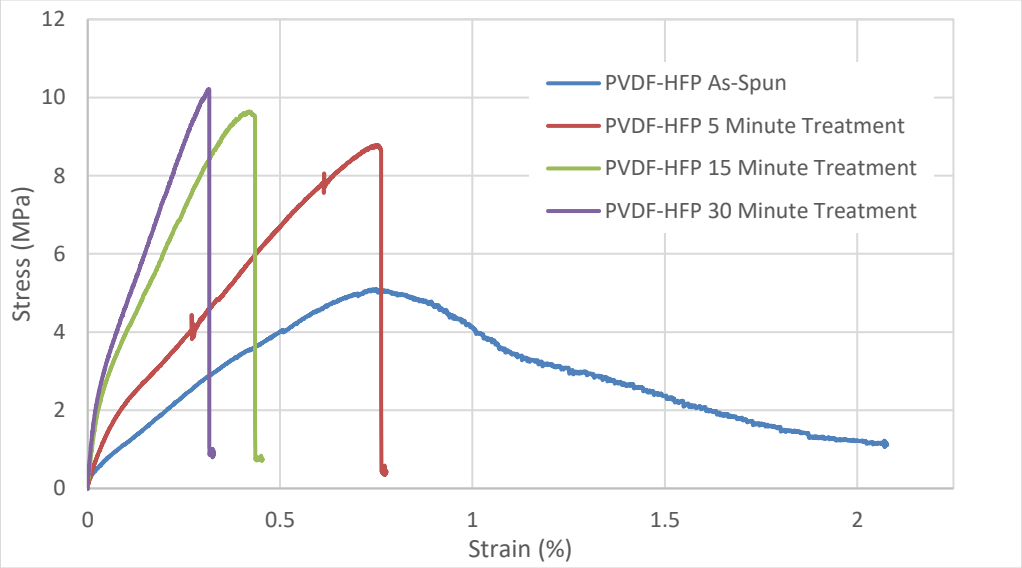

Figure 4.6 Tensile strength of homogenous PVDF-HFP samples after receiving heat treatment at 178 ºC for between 5 to 30 minutes

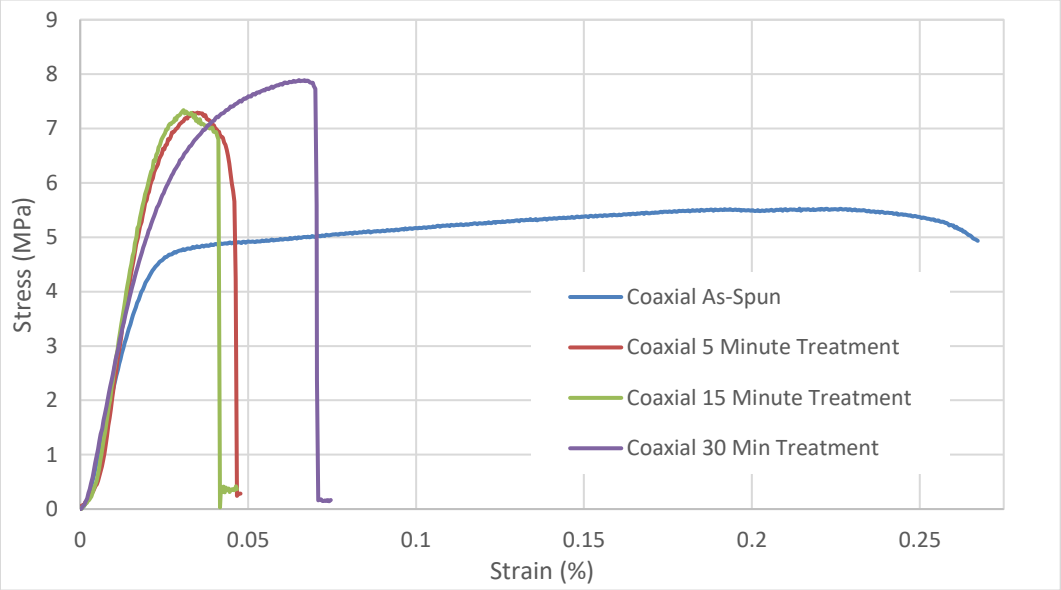

Figure 4.7 Tensile strength of coaxial PAN/PVDF-HFP samples after receiving heat treatment at 178 ºC for between 5 to 30 minutes

The coaxial mat therefore demonstrates a higher mechanical strength as-spun due to a combination of lower porosity, more significant inter-fiber bonding as-spun, and the incorporation of PAN which possesses a higher mechanical strength than PVDF-HFP [54]. However, post heat treatment, the coaxial mats demonstrate a lower ultimate tensile strength compared to the homogenous PVDF-HFP mats, despite the aforementioned factors. This likely indicates weaker inter-fiber bonds in the coaxial mats, as at higher levels of inter-fiber bonding, the properties of the bonds play a greater role in determining the mechanical strength of the mats than the individual fiber properties. [68, 73] This is likely a result of the outer sheath of PVDF-HFP present in the coaxial fibers being thinner than the homogenous PVDF-HFP fibers, resulting in less material being available for the inter-fiber bonds.

4.4.1 Performance Comparison

The physical characteristics of the homogenous PVDF-HFP and coaxial PAN/PVDF-HFP mats are compared below in **Table 3** to data reported in literature. The reported tensile strengths of PVDF based as-spun mats range between 2 and 7.58 MPa. As such, the heat treated PAN/PVDF-HFP mats

fabricated in this study successfully exceeded the mechanical strength of typical as-spun PVDF nanofiber.

Table 3 Performance Comparison of Electrospun Nanofiber Mats

Sample		Tensile Strength (MPa)	Porosity (%)	Ref.
Homogenous PVDF-HFP	As-Spun	5.02 ± 1.54	95.6 ± 10.4	This Study
	Heat Treated	10.38 ± 3.55	91.6 ± 13.9	
Coaxial PAN/PVDF	As-Spun	6.33 ± 0.53	79.4 ± 11.8	
	Heat Treated	7.72 ± 1.19	83.4 ± 23.1	
Celgard 2400	Transverse Direction, Typical	13.7	41	Industrial supplier
	Transverse Direction, Minimum	6.9		
	Machine Direction, Typical	139.3		
As-Spun PVDF		7.58	-	[36]
As-Spun PVDF		3.25	84.1	[74]
As-Spun PVDF-HFP		7.1	77.7 ± 1.0	[44]
Heat Treated PVDF		9.50	80.3	[74]
Dip-coated PVDF-HFP-DPA		11.2	72.8 ± 1.0	[44]
As-Spun Co-Spun PVDF-HFP/PI		2	-	[8]
Heat Treated Co-Spun PVDF-HFP/PI		7.5	73	[8]
Heat Treated Co-Spun PVDF-HFP+PI		6.78	80.1	[55]
Heat Treated Side-by-Side PVDF-HFP/PI		9.76	85.9	[55]
As-Spun Coaxial PPESK/PVDF		3.5	88	[58]
Hot-Pressed Coaxial PPESK/PVDF		23.2	65	[58]
As-Spun PI		12	87	[45]
Hot-Pressed PI		31	73	[45]

The nanofiber mats fabricated in this study also demonstrated exceptionally high porosities, meeting or exceeding most values reported in literature, and far exceeding the values reported for the commercial Celgard membrane. However, the coaxial mats prepared in this study fall short of the mechanical strengths reported for electrospun mats utilizing high-strength polymer components and the typical strength of the Celgard 2400 membrane in the machine direction. Further gains in performance could therefore be achieved by the incorporation of a high-strength polymer into the morphology developed in this study. Additionally, research has indicated that a minimum tensile strength of 13 MPa is required to allow a separator to consistently survive most commercial winding techniques for battery fabrication. **[12]** Therefore, further improvements to mechanical strength and

elongation at break are still necessary to allow the coaxial mats to serve as commercially viable separators.

4.5 Summary

The proposed method of combining conventional heat treatment with a coaxial morphology to improve mechanical strength without change in structure was performed in this chapter. Homogenous PVDF-HFP and coaxial PAN/PVDF-HFP nanofiber mats were produced with average fiber diameters of 1236 nm and 1499 nm, respectively. The coaxial mats demonstrated a beaded morphology which resulted in a decrease in porosity and an increase in mechanical strength, as spun.

The coaxial mats demonstrated no significant shrinkage when treated at temperatures up to 240 ºC for 20 minutes, while the homogenous mats experienced shrinkage of approximately 94% after being treated at 190 ºC. The coaxial mats displayed reductions in mat thickness of less than 8% after being treated at 178 ºC for up to 30 minutes and did not display the characteristic behaviour observed due to structural melting that was evident in the homogenous samples. Additionally, the coaxial mats possessed a lower porosity than the homogenous PVDF-HFP mats (79.4 $\pm$ 11.8% vs. 95.6 $\pm$ 10.4%, as-spun), but did not display a decrease in porosity after being treated at 178 ºC for 20 minutes. As such, it is clear that the reinforcing PAN core successfully prevented any significant changes in mat structure due to heat treatment.

Finally, the coaxial mats demonstrated a mechanical strength of 6.33 $\pm$ 0.53 MPa as-spun, and 7.72MPa after being treated at 178 ºC for 20 minutes. As such, the coaxial mats surpass the strength of the homogenous PVDF-HFP mats as-spun (5.02 $\pm$ 1.54 MPa) but falls short of the homogenous mats' mechanical strength after heat treatment (10.38 $\pm$ 3.55 MPa). The lower mechanical strength of the coaxial mats after heat treatment indicates that the inter-fiber bonding of the mats was weaker, likely due to an insufficient thickness in the outer PVDF-HFP sheath. The heat treated coaxial mats demonstrated mechanical strength superior to most as-spun and modified homogenous PVDF and PVDF-HFP nanofiber mats reported in literature, but were out-performed by nanofiber mats which incorporated high-strength polymers and the commercial celgard 2400 membrane. However, the heat treated coaxial mats demonstrated porosity equivalent to most nanofiber mats reported in literature and far exceeding that of the celgard 2400 membrane.

Overall, the coaxial nanofiber mats tested in this report fully succeeded in improving mechanical strength with no significant shrinkage or impact to mat structure, demonstrating the value of the proposed technique. However, further increases in mechanical strength are required to make this method commercially competitive. This could be accomplished by improving the strength of inter-fiber bonds and by replacing the reinforcing core material with a higher strength polymer.

Chapter 5
Conclusions and Recommendations

5.1 Conclusions

In this work, a coaxial PAN/PVDF-HFP structure was combined with thermal treatment to produce a novel method of improving the mechanical strength of nanofiber mats without incurring significant dimensional shrinkage. The coaxial PAN/PVDF-HFP mats showed no significant shrinkage when treated up to 240 ºC, while the homogenous PVDF-HFP mats shrunk by 94% when treated at 190 ºC. The coaxial fibers consistently experienced changes in thickness of less than 10% and no significant change in area when treated at 178 ºC for up to 30 minutes. The as-spun coaxial fibers showed a decrease in porosity compared to homogenous PVDF-HFP (95% to 79%) but remained much more porous than the commercial PP separator (41%). Coaxial samples heat treated at 178 ºC for 5 minutes demonstrated a mechanical strength of 7.72 MPa, a 22% increase compared to the as-spun coaxial fibers and a 54% increase compared to the as-spun homogenous PVDF-HFP. However, the mechanical strength of the heat treated coaxial fibers remains below that of the commercial Celgard 2400 separator (12.7 MPa) and the elongation at break for the mats decreased from 17.8% to 5.3% following heat treatment.

The proposed technique for combining coaxial fiber morphology with conventional heat treatment proved successful in significantly increasing the mechanical strength of the electrospun separator layers without loss of structure. The coaxial samples were able to achieve mechanical strength significantly higher than that of the as-spun homogenous nanofiber mats while maintaining the highly porous structure that allows them to perform more effectively than traditional commercial separators. However, the mechanical strength of the electrospun spun mats still needs to be improved further to allow them to be commercially viable.

5.2 Recommendations for Future Works

5.2.1 Finetuning of Coaxial Morphology

While the coaxial morphology in this report demonstrated the ability to increase mechanical performance with little to no effect on physical structure when paired with heat treatment, much work remains to improve performance. The effect of variations in outer wall thickness on the strength of the inter-fiber bonding in the nonwoven mats is not fully understood. Continuing work must be performed to identify the optimal outer wall thickness for maximizing mechanical strength in the samples. The elimination of the beaded morphology present in the coaxial samples would serve to further improve the porosity of the electrospun mats.

5.2.2 Comparison with Alternative Composite Morphologies

Similarly, while the coaxial morphology has proven effective when combined with conventional heat treatment, it remains difficult to control and optimize due to the large number of solution parameters and interactions which must be managed to produce high quality fibers. Similar results might therefore be achieved with less difficulty by using other composite nanofiber morphologies. Cross-electrospinning and side-by-side electrospinning, as described in Chapter 2, might be employed in a similar manner to coaxial electrospinning to achieve strong fiber-fiber bonding without significant change to physical structure. The performance of these different morphologies should be investigated alongside continuing coaxial experimentation to evaluate the comparative effectiveness of each.

5.2.3 Comparison with Alternative Material Selection

The selection of PAN and PVDF-HFP as the polymer components of the coaxial nanofibers studied in this report was due to the wide proliferation of each in the study of electrospun battery separators and due to their compatible thermal stabilities and melting points. However, it was observed that electrospun mats incorporating high-strength polymers such as PI and PPESK consistently reported high mechanical strength and good mechanical performance. As such, an effort should be made to incorporate these high-strength polymers into the methods explored in this report. In addition, further work should be performed to identify alternative surface materials to allow this technique to be applied in applications beyond battery research.

References

[1] G. I. Taylor, "Disintegration of water drops in an electric field, Proceedings of the Royal Society of London.," *Series A, Mathematical and Physical Sciences,* vol. 280, pp. 383-397, 1964.

[2] A. Yarin, S. Koombhongse and D. Reneker, "Taylor cone and jetting from liquid droplets in electrospinning of nanofibers," *Journal of Applied Physics,* vol. 90, no. 9, pp. 4836-4946, 2001.

[3] J. Doshi and D. H. Reneker, "Electrospinning process and applications of electrospun fibers," *Journal of Electrostatics,* vol. 35, no. 2, pp. 151-160, 1995.

[4] J. Bao, L. Clarke and R. Gorga, "Effect of constrained annealing on the mechanical properties of electrospun poly(ethylene oxide) webs containing multiwalled carbon nanotubes," *Journal of Polymer Science. Part B, Polymer Physics.,* vol. 54, no. 8, pp. 787-796, 2016.

[5] D. H. Reneker and I. Chun, "Nanometre diameter fibres of polymer, produced by electrospinning," *Nanotechnology,* vol. 7, no. 3, pp. 216-223, 1996.

[6] L. Persano, A. Camposeo, C. Tekmen and D. Pisignano, "Industrial Upscaling of Electrospinning and Applications of Polymer Nanofibers: A Review," *Macromolecular Materials and Engineering,* vol. 298, no. 5, pp. 504-520, 2013.

[7] F.-L. Zhou, r.-H. Gong and I. Porat, "Needle and needleless electrospinning for nanofibers," *Journal of Applied Polymer Science,* vol. 115, no. 5, pp. 2591-2598, 2010.

[8] W. Chen, Y. Liu, Y. Ma, J. Liu and X. Lie, "Improved performance of PVdF-HFP/PI nanofiber membrane for lithium ion battery separator prepared by a bicomponent cross-electrospinning method," *Materials Letters,* vol. 133, pp. 67-70, 2014.

[9] T. T. T. Nguyen, O. H. Chung and J. S. Park, "Coaxial electrospun poly(lactic acid)/chitosan (core/shell) composite nanofibers and their antibacterial activity," *Carbohydrate Polymers,* vol. 86, no. 4, pp. 1799-1806, 2011.

[10] R. Givehchi, Q. Li and Z. Tan, "Quality factors of PVA nanofibrous filters for airborne particles in the size range of 10–125 nm," *Fuel (Guildford),* vol. 181, pp. 1273-1280, 2016.

[11] J. Ahne, Q. Li, E. Croiset and Z. Tan, "Electrospun cellulose acetate nanofibers for airborne nanoparticle filtration," *Textile Research Journal,* vol. 89, no. 15, pp. 3137-3149, 2019.

[12] Y. Li, Q. Li and Z. Tan, "A review of electrospun nanofiber-based separators for rechargeable lithium-ion batteries," *Journal of Power Sources,* vol. 443, p. 227262, 2019.

[13] R. Givehchi, B. Du, M. Razavi, Z. Tan and J. Siegel, "Performance of nanofibrous media in portable air cleaners," *Aerosol Science and Technology,* vol. 55, no. 7, pp. 805-816, 2021.

[14] Y. Li, H. Yu, Y. Zhang, N. Zhou and Z. Tan, "Kinetics and characterization of preparing conductive nanofibrous membrane by In-situ polymerization of Polypyrrole on electrospun nanofibers," *Chemical Engineering Journal,* vol. 433, p. 133531, 2022.

[15] R. Givehchi, Q. Li and Z. Tan, "Filtration of sub-3.3 nm tungsten oxide particles using nanofibrous filters," *Materials,* vol. 11, no. 8, p. 1277, 2018.

[16] R. Givehchi and Z. Tan, "Filtration of NaCl and WOx nanoparticles using wire screens and nanofibrous filters," University of Waterloo, 2016.

[17] E. Gao, "Multiple Tools for Automated Nanofiber Characterization by Image Processing," University of Waterloo, 2022.

[18] Y. Li and Z. Tan, "Polypyrrole-based Nanofibrous Membrane Separator for Lithium-ion Battery," University of Waterloo, 2021.

[19] Y. Li, Y. Zhang, N. Zhou, H. Yu and Z. Tan, "Electrospun-nanofibrous Redox-active separator for enhancing the capacity of Lithium-ion batteries," *Chemical Engineering Science,* vol. 260, p. 117873, 2022.

[20] R. Givehchi and Z. Tan, "An overview of airborne nanoparticle filtration and thermal rebound theory," *Aerosol and Air Quality Research,* vol. 14, no. 1, pp. 46-63, 2014.

[21] M. Khodabakhsdi, J. Z. Wen and Z. Tan, "Coefficient of restitution for silver nanoparticles colliding on a wet silver substrate," *Applied Surface Science,* vol. 554, p. 149607, 2021.

[22] M. Razavi, Z. Tan and Z. Pan, "A Comprehensive Model for Filtration and Adsorption of Intermediate Nanoparticles," University of Waterloo, 2020.

[23] M. Khodabakshi, J. Z. Wen and Z. Tan, "Coefficient of restitution of sub-10 nm silver nanoparticles on an adhesive surface under repulsive and sticky conditions: Silver nanoparticle collisions on an adhesive surface," *The European Physical Journal. D, Atomic, Molecular, and optical physics.*, vol. 76, no. 9, 2022.

[24] Y. Zhang, Y. Huang, Y. Li, H. Yu and Z. Tan, "Free energy barrier in wetting parallel-structured surfaces," *Colloids and Surfaces,* vol. 655, p. 130214, 2022.

[25] H. Jin, S. Li, H. Yu, L. Yuan, F. Zhou and Z. Tan, "Filtration of dust particles in underground coal mines," *Powder Technology,* vol. 423, 2023.

[26] X. Zhang, L. Ji, O. Toprakci, Y. Liang and M. Alcoutlabi, "Electrospun Nanofiber-based Anodes, Cathodes, and Separators for Advanced Lithium-Ion Batteries," *Polymer Reviews,* vol. 51, no. 3, pp. 239-264, 2011.

[27] Z. Li, J.-W. Zhang, L.-G. Yu and J.-W. Zhang, "Electrospun porous nanofibers for electrochemical energy storage," *Journal of Materials Science,* vol. 52, no. 11, pp. 6173-6195, 2017.

[28] J.-W. Jung, C.-L. Lee, S. Yu and I.-D. Kim, "Electrospun nanofibers as a platform for advanced secondary batteries: a comprehensive review," *Journal of Materials Chemistry,* vol. 4, no. 3, pp. 73-75, 2016.

[29] S. S. Zhang, "A review on the separators of liquid electrolyte Li-ion batteries," *Journal of Power Sources,* vol. 164, no. 1, pp. 351-364, 2007.

[30] V. Deimede and C. Elmasides, "Separators for Lithium-Ion Batteries: A Review on the Production Processes and Recent Developments," *Energy Technology,* vol. 3, no. 5, pp. 453-468, 2015.

[31] X. Huang, "Separator technologies for lithium-ion batteries," *Journal of solid state electrochemistry,* vol. 15, no. 4, pp. 649-662, 2011.

[32] K. Bicy, A. B. Gueye, D. rouxel, N. Kalarikkal and S. Thomas, "Lithium-ion battery separators based on electrospun PVDF: A review," *Surfaces and Interfaces,* vol. 31, p. 101977, 2022.

[33] H. Lee, M. Yanilmaz, O. Toprakci, K. Fu and X. Zhang, "A review of recent developments in membrane separators for rechargeable lithium-ion batteries," *Energy & Environmental Science,* vol. 7, no. 12, pp. 3857-3886, 2014.

[34] C. Shi, P. Zhang, S. Huang, X. He, P. Yang, D. Wu, D. Sun and J. Zhao, "Functional separator consisted of polyimide nonwoven fabrics and polyethylene coating layer for lithium-ion batteries," *Journal of Power Sources,* vol. 298, pp. 158-165, 2015.

[35] S. J. Lee, S. H. Oh, J. Liu, S. Soker, A. Atala and J. J. Yoo, "The use of thermal treatments to enhance the mechanical properties of electrospun poly(ε-caprolactone) scaffolds," *Biomaterials,* vol. 29, no. 10, pp. 1422-1430, 2008.

[36] S. W. Choi, J. R. Kim, Y. R. Ahn, S. M. Jo and E. J. Cairns, "Characterization of Electrospun PVdF Fiber-Based Polymer Electrolytes," *Chemistry of Materials,* vol. 19, no. 1, pp. 104-115, 2007.

[37] H. Widiyandari, A. Purwanto and S. A. Widyanto, "Polyvinilidine fluoride (PVDF) nanofiber membrane for Li-ion rechargeable battery separator," *Journal of Physics,* vol. 817, no. 1, p. 12013, 2017.

[38] K. Castkova, J. Kastyl, D. Sobola, J. Petrus, E. Stastna, D. Riha and P. Tofel, "Structure–Properties Relationship of Electrospun PVDF Fibers," *Nanomaterials,* vol. 10, no. 6, p. 1221, 2020.

[39] B. Zaarour, L. Zhu and X. Jin, "Controlling the surface structure, mechanical properties, crystallinity, and piezoelectric properties of electrospun PVDF nanofibers by maneuvering molecular weight," *Soft Materials,* vol. 17, no. 2, pp. 181-189, 2019.

[40] Y.-E. Miao, G.-N. Zhu, H. Hou, Y.-Y. Xia and T. Liu, "Electrospun polyimide nanofiber-based nonwoven separators for lithium-ion batteries," *Journal of Power Sources,* vol. 226, pp. 82-86, 2013.

[41] C. Cheng, C. Juan, F. Chen, P. hu, X.-F. Wu, D. H. Reneker and H. Hou, "High-Strength and High-Toughness polyimide nanofibers: Synthesis and Characterization," *Journal of Applied Polymer Science,* vol. 116, no. 3, pp. 1581-1586, 2010.

[42] S. Chen, P. Hu, A. Greiner, C. Cheng, H. Cheng, F. Chen and H. Hou, "Electrospun nanofiber belts made from high performance copolyimide," *Nanotechnology,* vol. 19, no. 1, pp. 015604-015604, 2008.

[43] X. Huan, "A lithium-ion battery separator prepared using a phase inversion process," *Journal of Power Sources,* vol. 216, pp. 216-221, 2012.

[44] C. Shi, J. Dai, S. Huang, C. Li, X. Shen, P. Zhang, D. Wu, D. Sun and J. Zhao, "A simple method to prepare a polydopamine modified core-shell structure composite separator for application in high-safety lithium-ion batteries," *Journal of Membrane Science,* vol. 518, pp. 168-177, 2016.

[45] W. Jiang, Z. Liu, Q. Kong, J. Yao, C. H. P. Zhang and G. Cui, "A high temperature operating nanofibrous polyimide separator in Li-ion battery," *Solid State Ionics,* vol. 232, pp. 44-48, 2013.

[46] S. J. Lee, S. H. Oh, j. Liu, S. Soker, A. Atala and J. J. Yoo, "The use of thermal treatments to enhance the mechanical properties of electrospun poly(ε-caprolactone) scaffolds," *Biomaterials,* vol. 29, no. 10, pp. 1422-1430, 2008.

[47] O. Rozent, V. V. Beilin, G. E. Shter, G. S. Grader and J. Jones, "Deformation Control During Thermal Treatment of Electrospun PbZr0.52Ti0.48O3 Nanofiber Mats," *Journal of the American Ceramic Society,* vol. 99, no. 5, pp. 1550-1556, 2016.

[48] H. Li, C. Zhu, J. Xue, Q. Ke and Y. Xia, "Enhancing the Mechanical Properties of Electrospun Nanofiber Mats through Controllable Welding at the Cross Points," *Macromolecular Rapid Communications,* vol. 38, no. 9, p. 1600723, 2017.

[49] y. Zhai, N. Wang, X. Mao, Y. Si, J. Yu, S. S. Al-Deyab, M. El-Newehy and B. Ding, "Sandwich-structured PVdF/PMIA/PVdF nanofibrous separators with robust mechanical strength and thermal stability for lithium ion batteries," *Journal of Materials Chemistry,* vol. 2, no. 35, pp. 14511-14518, 2014.

[50] J. Liu, Y. Liu, W. yang, Q. Ren, F. Li and Z. Huang, "Lithium ion battery separator with high performance and high safety enabled by tri-layered SiO2@PI/m-PE/SiO2@PI nanofiber composite membrane," *Journal of Power Sources,* vol. 396, pp. 265-275, 2018.

[51] D. Wu, C. Shi, S. Huang, X. Qiu, H. Wang, Z. Zhan, P. Zhang, J. Zhao, D. Sun and L. Lin, "Electrospun Nanofibers for Sandwiched Polyimide/Poly (vinylidene fluoride)/Polyimide Separators with the Thermal Shutdown Function," *Electrochimica acta,* vol. 176, pp. 727-734, 2015.

[52] Q. Shi, M. Yu, X. Zhou, Y. Yan and C. Wan, "Structure and performance of porous polymer electrolytes based on P(VDF-HFP) for lithium ion batteries," *Journal of Power Sources,* vol. 103, no. 2, pp. 286-292, 2002.

[53] m. Kundu, C. M. Costa, J. Dias, A. Maceiras, J. L. Vilas and S. Lanceros-Mendez, "On the Relevance of the Polar β-Phase of Poly(vinylidene fluoride) for High Performance Lithium-Ion Battery Separators," *Journal of Physical Chemistry,* vol. 121, no. 47, pp. 26216-26225, 2017.

[54] Y. Zhu, M. yin, H. liu, B. Na, R. Lv, B. Wang and Y. Huang, "Modification and characterization of electrospun poly (vinylidene fluoride)/poly (acrylonitrile) blend separator membranes," *Composites,* vol. 112, pp. 31-37, 2017.

[55] M. Cai, D. Yuan, X. Zhang, Y. Pu, X. Liu, H. He, L. Zhang and X. Ning, "Lithium ion battery separator with improved performance via side-by-side bicomponent electrospinning of PVDF-HFP/PI followed by 3D thermal crosslinking," *Journal of Power Sources,* vol. 461, p. 228123, 2020.

[56] F. Huang, Y. Xu, B. Peng, Y. Su, F. Jiang, Y.-L. Hsieh and Q. Wei, "Coaxial Electrospun Cellulose-Core Fluoropolymer-Shell Fibrous Membrane from Recycled Cigarette Filter as

Separator for High Performance Lithium-Ion Battery," *ACS Sustainable Chemistry & Engineering,* vol. 3, no. 5, pp. 932-940, 2015.

[57] X. Jiang, L. Xiao, X. Ai, H. Yang and Y. Cao, "A novel bifunctional thermo-sensitive poly(lactic acid)@poly(butylene succinate) core–shell fibrous separator prepared by a coaxial electrospinning route for safe lithium-ion batteries," *Journal of Materials Chemistry,* vol. 5, no. 44, pp. 23238-23242, 2017.

[58] W. Gong, X. Wang, Z. Li, J. Gu, S. Ruan and C. Shen, "A high-strength PPESK/PVDF fibrous membrane prepared by coaxial electrospinning for lithium-ion battery separator," *High Performance Polymers,* vol. 31, no. 8, pp. 948-958, 2019.

[59] M. Yanilmaz, J. Zhu, y. Lu, Y. Ge and X. Zhang, "High-strength, thermally stable nylon 6,6 composite nanofiber separators for lithium-ion batteries," *Journal of Material Science,* vol. 52, no. 9, pp. 5232-5241, 2017.

[60] H.-l. Chen and X.-n. Jiao, "Preparation and characterization of Polyvinylidene fluoride/Octaphenyl-Polyhedral oligomeric silsesquioxane hybrid Lithium-ion battery separators by electrospinning," *Solid State Ionics,* vol. 310, pp. 134-142, 2017.

[61] R. Givehchi, Q. Li and Z. Tan, "Quality factors of PVA nanofibrous filters for airborne particles in the size range of 10–125 nm," *Fuel,* vol. 181, pp. 1273-1280, 2016.

[62] A. Moghe and B. Gupta, "Co-axial Electrospinning for Nanofiber Structures: Preparation and Applications," *Polymer Reviews,* vol. 48, no. 2, pp. 353-377, 2008.

[63] M. Mckee, G. Wilkes, R. Colby and T. Long, "Correlations of Solution Rheology with Electrospun Fiber Formation of Linear and Branched Polyesters," *Macromolecules,* vol. 37, no. 5, pp. 1760-1767, 2004.

[64] S. Shenoy, D. Bates, H. Frisch and G. Wnek, "Role of chain entanglements on fiber formation during electrospinning of polymer solutions: good solvent, non-specific polymer–polymer interaction limit," *Polymer (Guilford),* vol. 46, no. 10, pp. 3372-3384, 2005.

[65] C. Zhang, X. Yuan, L. Wu, Y. Han and J. Sheng, "Study on morphology of electrospun poly(vinyl alcohol) mats," *European Polymer Journal,* vol. 41, no. 3, pp. 423-432, 2005.

[66] M. Wang, J. Yu, d. Kaplan and G. Rutledge, "Production of Submicron Diameter Silk Fibers under Benign Processing Conditions by Two-Fluid Electrospinning," *Macromolecules,* vol. 39, no. 3, pp. 1102-1107, 2006.

[67] Z. Lu, W. Hu, F. Xie and Y. Hao, "Highly improved mechanical strength of aramid paper composite via a bridge of cellulose nanofiber," *Cellulose (London),* vol. 24, no. 7, pp. 2827-2835, 2017.

[68] K. Wei, T. Vigo and B. Goswami, "Structure-property relationships of thermally bonded polypropylene nonwovens," *Journal of Applied Polymer Science,* vol. 30, no. 4, pp. 1523-1534, 1985.

[69] E. Ciprani, M. Zanetti, P. Bracco, V. Brunella, M. Luda and L. Costa, "Crosslinking and carbonization processes in PAN films and nanofibers," *Polymer Degradation and Stability,* vol. 123, pp. 178-188, 2016.

[70] A. Gupta, D. Paliwal and P. Bajaj, "Melting Behavior of Acrylonitrile Polymers," *Journal of Applied Polymer Science,* vol. 70, no. 13, pp. 2703-2709, 1998.

[71] O. Elishav, V. Beilin, O. Rozent, G. Shter and G. Grader, "Thermal Shrinkage of Electrospun PVP Nanofibers," *Journal of Polymer Science,* vol. 56, no. 3, pp. 248-254, 2018.

[72] P. Chavoshnejad and M. Razavi, "Effect of the Interfiber Bonding on the Mechanical Behaviour of Electrospun Fibrous Mats," *Scientific Reports,* vol. 10, no. 1, pp. 7709-7709, 2020.

[73] T. U. Rashid, R. E. Gorga and W. E. Krause, "Mechanical Properties of Electrospun Fibers—A Critical Review," *Advanced Engineering Materials,* vol. 23, no. 9, p. 2100153, 2021.

[74] Y. Liang, S. Cheng, J. Zhao, C. Zhang, S. Sun, N. Zhou, Y. Qiu and X. Zhang, "Heat treatment of electrospun Polyvinylidene fluoride fibrous membrane separators for rechargeable lithium-ion batteries," *Journal of Power Sources,* vol. 240, pp. 204-211, 2013.

[75] O. Rozent, V. Beilin, G. Shter, G. Grader and J. Jones, "Deformation Control During Thermal Treatment of Electrospun PbZr0.52Ti0.48O3 Nanofiber Mats," *Journal of American Ceramic Society*, vol. 99, no. 5, pp. 1550-1556, 2016.

[76] C. Sun, Y. Boluk and C. Ayranci, "Investigation of nanofiber nonwoven meshes produced by electrospinning of cellulose nanocrystal suspensions in cellulose acetate solutions," *Cellulose*, vol. 22, no. 4, pp. 2457-2470, 2015.

[77] D. Grove, P. Desai and A. Abhiraman, "Exploratory experiments in the conversion of plasticized melt spun PAN-based precursors to carbon fibers," *Carbon*, vol. 26, no. 3, pp. 403-411, 1988.

[78] B. Frushour, "Melting behavior of polyacrylonitrile copolymers," *Polymer Bulletin*, vol. 11, no. 4, pp. 375-382, 1984.

[79] J. Ahne, Q. Li, E. Croiset and Z. Tan, "Electrospun cellulose acetate nanofibers for airborne nanoparticle filtration," *Textile Research Journal*, vol. 89, no. 15, pp. 3137-3149, 2019.

[80] R. Givehchi and Z. Tan, "An overview of airborne nanoparticle filtration and thermal rebound theory," *Aerosol and Air Quality Research*, vol. 14, no. 1, pp. 46-63, 2014.

Appendix A
Behaviour of Homogenous and Coaxial Nanofiber Mats under Increasing Treatment Temperature

A.1 Introduction

It was deemed necessary to investigate the effect of different heat treatment programs on the binding between homogenous and coaxial fibers. This will allow for the identification of the ideal treatment temperature to be used to produce the strongest possible inter-fiber bonds.

A.2 Experimental

A.2.1 Materials

Polyacrylonitrile (PAN, Mw 150000), Polyvinylidene fluoride-hexafluoropropylene (PVDF-HFP, Mw 455000), Dimethylformamide (DMF, 99.8% purity), and n-butyl-alcohol (N-butanol, 99.5% purity) were purchased from Sigma Aldrich (Canada). Acetone (99.8% purity) was purchased from Fisher Scientific (USA). All chemicals were used as purchased without modification.

A.2.2 Fabrication of Samples

Homogenous PVDF-HFP nanofiber mats were produced using the following method. PVDF-HFP polymer was dissolved in a solvent mixture comprised of acetone and DMF in a 7:3 ratio by mass to create a precursor solution of 12% mass concentration. This solution was extruded through a 21-gauge syringe at a distance of 11cm onto a rotational drum collector rotating at 20rpm and coated in a non-stick aluminium foil substrate. A voltage of 9kV was applied to the solution at a constant flowrate of 1.25mL/hr. All nanofiber production was carried out between 21 to 23 degrees Celsius and 20% to 45% relative humidity.

Coaxial PAN/PVDF-HFP nanofiber mats were produced using the following method. PVDF-HFP polymer was dissolved in a solvent mixture comprised of acetone and DMF in a 3:7 ratio by mass to create a sheath precursor solution of 12% mass concentration. PAN polymer was dissolved in pure DMF to create a 10% mass concentration solution. The PAN solution was extruded within the interior 22-gauge syringe at a rate of 0.6mL/hr, while the PVDF-HFP solution was extruded between the interior 22-gauge syringe and an exterior 15-gauge syringe at a rate of 0.9mL/hr. A voltage of 7.5kV was applied to the syringe at 11cm from a drum collector rotating at 20rpm. All nanofiber production was carried out between 21 to 23 degrees Celsius and 20% to 45% relative humidity.

Samples were divided into approximately 2cm by 2cm squares in batches of five. These samples were then heat treated in batches of 5 in an isothermal oven (Precision Compact Oven, Thermo Fisher Scientific, USA). Samples were treated for 20 minutes at between 140 ºC to 180 ºC.

A.2.3 Characterization of Samples

The morphology of the samples was analyzed using an ESEM (Quanta Feg 250 ESEM, FEI, USA) to collect high-resolution photos of the samples.

The tensile strength of the samples was evaluated using a UTM device (5548 Micro-Tester, Instron, USA). The samples were tested until failure. The stress and strain were calculated using the data from the UTM and the measured dimensions of the samples.

A.3 Results and Discussions

The morphologies of the homogenous PVDF-HFP nanofiber mats after undergoing heat treatment at between 140 ºC to 170 ºC are shown in Figure A.5.1 The samples treated at 180 ºC experienced destructive levels of shrinkage. As can been seen from the figure, fusing of fibers at fiber junctions is already evident in the sample treated at 140 ºC. However, further significant changes in morphology are only evident in the sample treated at 170 ºC. It is at this point that the fibers show significant melting behaviour, as they begin to flatten and lose their cylindrical fiber structure and show increased degrees of fiber fusing. This agrees with the results reported by Shi *et al.* [44] which observed significant melting behaviour onset in a pure PVDF-HFP nanofiber sample after being treated at 170 ºC for 30 minutes.

It is therefore evident that the greatest degree of stable melting behaviour occurs in the region immediately surrounding 170 ºC. With temperatures significantly below this demonstrating less complete melting behaviour, and temperatures significantly above this demonstrating destructive melting and shrinking behaviour which renders the PVDF-HFP samples unusable.

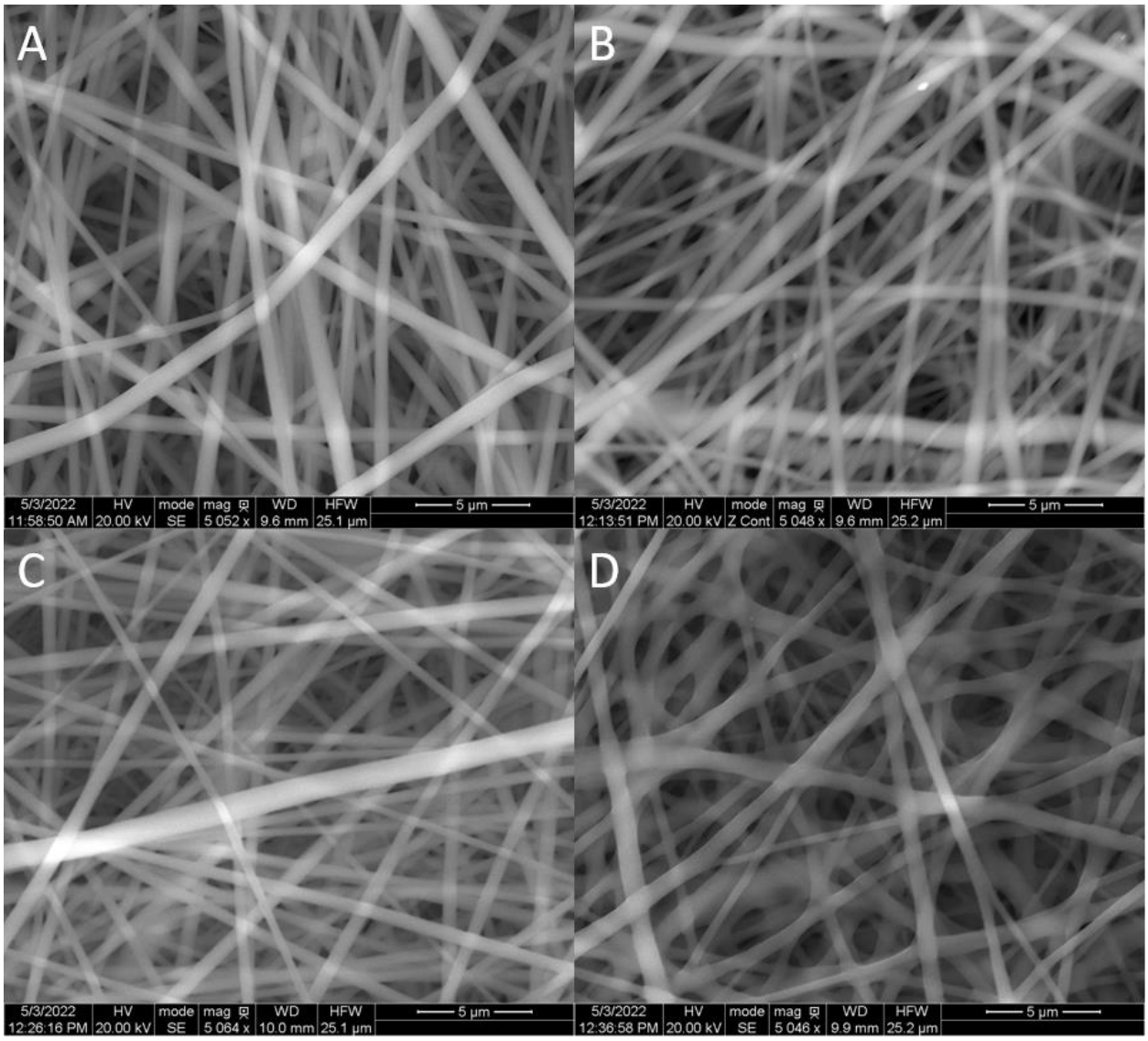

Figure A.5.1 PVDF-HFP Nanofiber mats after being treated for 20 minutes at A) 140 ºC, B) 150 ºC, C) 160 ºC, and D) 170 ºC

The mechanical strengths of homogenous PVDF-HFP and coaxial PAN/PVDF-HFP nanofiber mats after undergoing heat treatment for 20 minutes at temperatures between 150 ºC and 170 ºC are shown in Figure A.5.2 and Figure A.5.3, respectively. As can be seen in the figure, the mechanical strength and elongation at break of the homogenous PVDF-HFP samples are quite similar when treated at 150 ºC and 160 ºC, but mechanical strength is increased significantly in the sample treated at 170 ºC. This

behaviour corresponds strongly with the significantly more prevalent melting behaviour evident in Figure A.5.1.

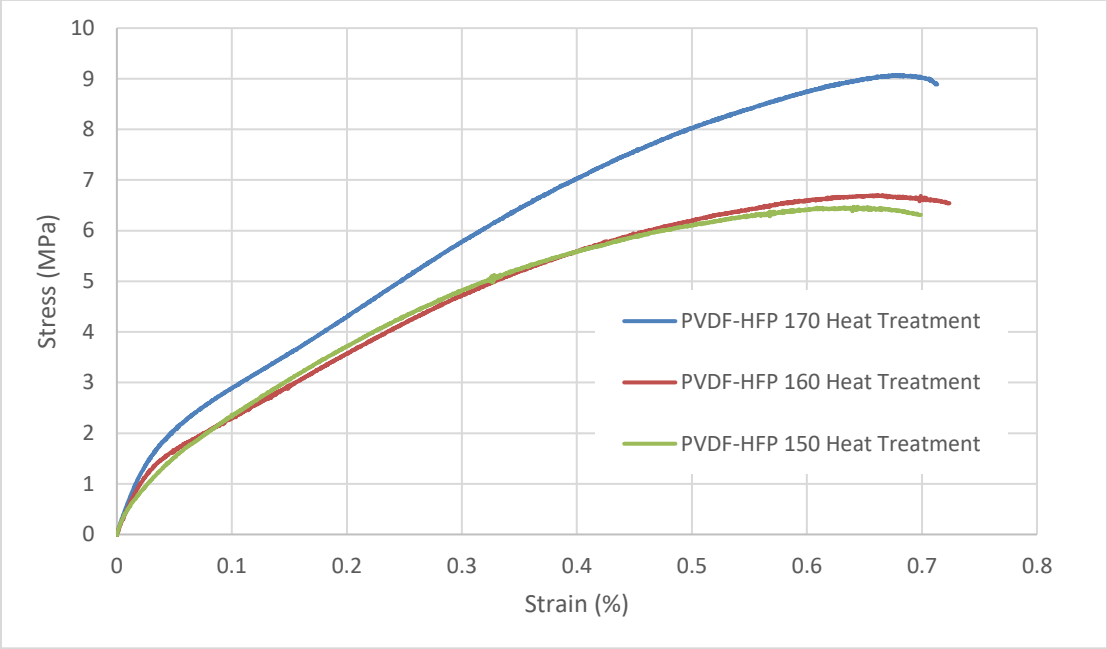

Figure A.5.2 Tensile strength of homogenous PVDF-HFP samples after heat treatment at 150º-170 ºC for 20 minutes

The greatest tensile strength among the coaxial samples is still seen in the sample treated at 170 ºC, however the major jump in strength occurred between the samples treated at 150 ºC and 160 ºC. The coaxial samples also demonstrate significantly more developed elastic deformation regions (with steep slopes), significantly lower overall tensile strength, and significantly reduced elongation at break. The steeper slope of the elastic region of deformation is most likely due to the incorporation of PAN which possesses a higher mechanical strength than PVDF-HFP. [54] However, the lower overall strength is likely indicative of weaker inter-fiber bonds in the coaxial mats, as the properties of the inter-fiber bonds play a greater role in determining the mechanical strength of the mats than the individual fiber properties at high levels of bonding. [68, 73] The relatively small difference in strength between the samples heated at 160 ºC and 170 ºC also indicates that the strength of the mat may be affected by the thickness of the relatively thin outer sheath of PVDF-HFP in coaxial fibers, as less heat is needed to induce significant melting behaviour. It is therefore evident that higher treatment temperatures result in stronger inter-fiber bonds.

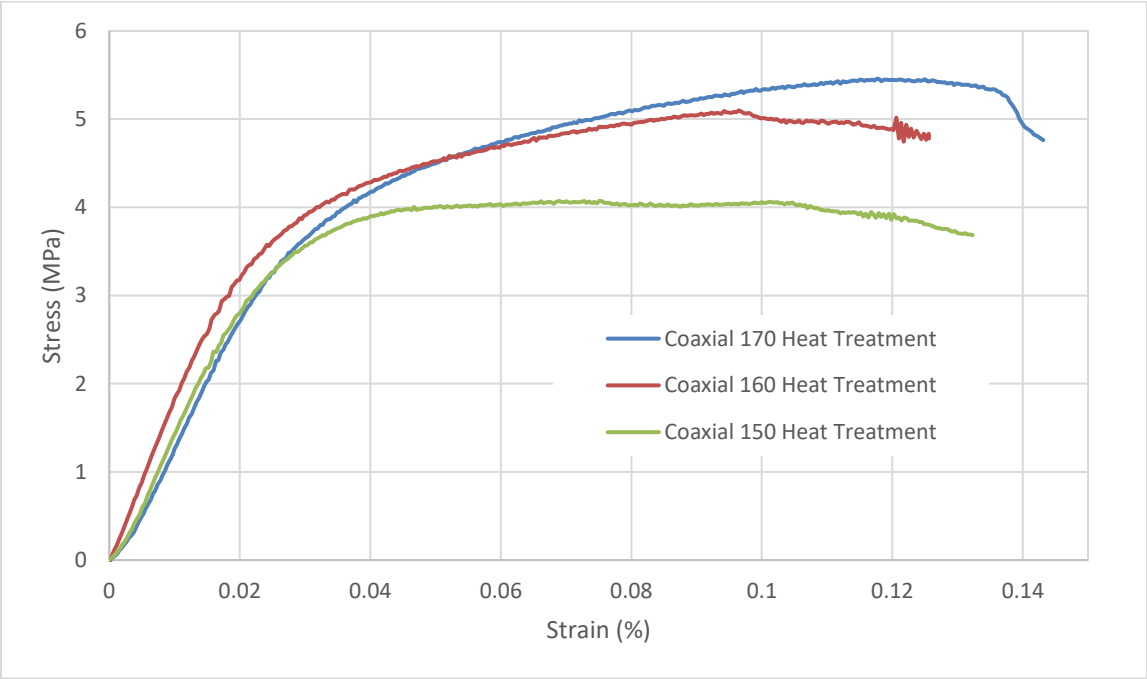

Figure A.5.3 Tensile strength of coaxial PAN/PVDF-HFP samples after heat treatment at 150º-170 ºC for 20 minutes

A.4 Conclusions

Homogenous and coaxial nanofiber mats were treated at temperatures between 140 ºC and 180 ºC in this appendix. It was evident from the SEM analysis that the greatest melting behaviour occurred at 170 ºC with higher treatment temperatures resulting in the destruction of the samples. This observation was corroborated by the tensile testing of the heat treated samples, which showed that maximum mechanical strength occurred after treatment at 170 ºC for both the homogenous and coaxial samples. However, the effect of the heat treatment appeared diminished on the coaxial samples, with both a lower overall ultimate tensile strength and a smaller difference in mechanical strength between samples treated at different temperatures. This was hypothesized to be a result of the outer layer of PVDF-HFP present in the coaxial samples being thinner than the pure PVDF-HFP nanofibers, resulting in weaker inter-fiber bonds. However, it remains clear that maximum mechanical strength occurs at temperatures in the region above 170 ºC and below 180 ºC, as more significant melting behaviour yields higher strength.